Accepted Manuscript

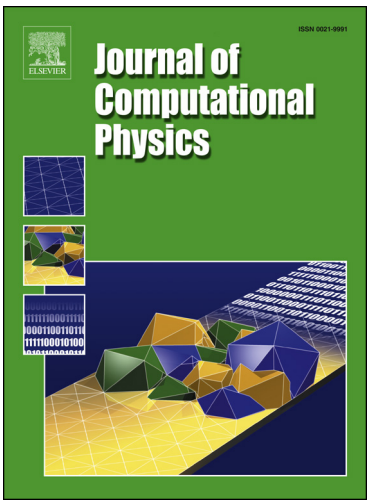

Simulation of transcritical fluid jets using the PC-SAFT EoS

C. Rodriguez, A. Vidal, P. Koukouvinis, M. Gavaises, M.A. McHugh

PII: S0021-9991(18)30491-1
DOI: https://doi.org/10.1016/j.jcp.2018.07.030
Reference: YJCPH 8155

To appear in: *Journal of Computational Physics*

Received date: 1 February 2018
Revised date: 11 July 2018
Accepted date: 12 July 2018

Please cite this article in press as: C. Rodriguez et al., Simulation of transcritical fluid jets using the PC-SAFT EoS, *J. Comput. Phys.* (2018), https://doi.org/10.1016/j.jcp.2018.07.030

Highlights

- A numerical framework to simulate transcritical and supercritical flows utilising the compressible form of the Navier–Stokes equations coupled with the Perturbed Chain Statistical Associating Fluid Theory (PC-SAFT) equation of state (EoS) is presented.
- Both conservative and quasi-conservative formulations have been tested.
- Advection test cases and shock tube problems are included to show the overall performance of the developed framework.
- Two-dimensional simulations of nitrogen and dodecane jets are presented to demonstrate the multidimensional capability of the developed model.

Simulation of transcritical fluid jets using the PC-SAFT EoS

C. Rodriguez [a,*], A. Vidal [a], P. Koukouvinis [a], M. Gavaises [a], M. A. McHugh [b]

[a] *School of Mathematics, Computer Science & Engineering, Department of Mechanical Engineering & Aeronautics, City University London, Northampton Square EC1V 0HB, United Kingdom*

[b] *Department of Chemical and Life Science Engineering, 601 West Main Street, Richmond, VA 23284, USA*

**Corresponding author: Carlos.Rodriguez@city.ac.uk*

Abstract

The present paper describes a numerical framework to simulate transcritical and supercritical flows utilising the compressible form of the Navier-Stokes equations coupled with the Perturbed Chain Statistical Associating Fluid Theory (PC-SAFT) equation of state (EoS); both conservative and quasi-conservative formulations have been tested. This molecular model is an alternative to cubic EoS which show low accuracy computing the thermodynamic properties of hydrocarbons at temperatures typical for high pressure injection systems. Liquid density, compressibility, speed of sound, vapour pressures and density derivatives are calculated with more precision when compared to cubic EoS. Advection test cases and shock tube problems are included to show the overall performance of the developed framework employing both formulations. Additionally, two-dimensional simulations of nitrogen and dodecane jets are presented to demonstrate the multidimensional capability of the developed model.

Keywords: Supercritical, transcritical, PC-SAFT EoS, double-flux model, Riemann problem

Nomenclature

List of abbreviations

AAD	Average Absolute Deviation
CFD	Computational Fluid Dynamics
CFL	Courant–Friedrichs–Lewy
ENO	Essentially Non-Oscillatory
EoS	Equation of State
FC	Fully Conservative
HLLC	Harten-Lax-van Leer-Contact
LES	Large Eddy Simulation
PR	Peng-Robinson
PC-SAFT	Perturbed Chain Statistical Associating Fluid Theory
QC	Quasi-Conservative
RK2	Second-order Runge–Kutta
SRK	Soave-Redlich-Kwong

SSP-RK3	Third-order strong-stability-preserving Runge–Kutta
TVD	Total Variation Diminishing
WENO	Weighted Essentially Non-Oscillatory

List of Symbols

$\tilde{a}^{res}$	Reduced Helmholtz free energy [-]
c	Sound speed [m s^{-1}]
d	Temperature-dependent segment diameter [Å]
g	Radial distribution function [-]
I	Integrals of the perturbation theory [-]
k_B	Boltzmann constant [J/K]
m	Number of segments per chain [-]
$\overline{m}$	Mean segment number in the system [-]
p	Pressure [Pa]
R	Gas constant [J mol^{-1} K^{-1}]
T	Temperature [K]
x_i	Mole fraction of component i [-]
Z	Compressibility factor [-]
$\mathbf{U}$	Conservative variable vector
$\mathbf{F}$	x-convective flux vector
$\mathbf{G}$	y-convective flux vector
$\mathbf{F}_\mathbf{V}$	x-diffusive flux vector
$\mathbf{G}_\mathbf{V}$	y-diffusive flux vector

Greek Letters

ε	Depth of pair potential [J]
η	Packing fraction [-]
ρ	Density [kg/m^3]
ρ_m	Total number density of molecules [1/Å^3]
σ_d	Segment diameter [Å]

Superscripts

disp	Contribution due to dispersive attraction
hc	Residual contribution of hard-chain system
hs	Residual contribution of hard-sphere system
id	Ideal gas contribution

1. Introduction

Transcritical and supercritical states occur in modern combustion engines that operate at pressures higher than the critical pressure of the fuels utilised. In Diesel engines for example, the liquid fuel is injected into air at pressure and temperature conditions higher than the critical point of the fuel [1]. The liquid injection temperature is lower than the fuel critical temperature but as the liquid is heated, it may reach supercritical temperature before full vaporisation. This is known as a transcritical injection. Similarly, in liquid rocket engines, cryogenic propellants are injected into chambers under conditions that exceed the critical pressure and temperature of the propellants.

A single-species fluid or a mixture reaches a supercritical state when the pressure and temperature surpass its critical properties. In the critical region, repulsive interactions overcome the surface tension resulting in the existence of a single-phase that exhibits properties of both gases and liquids (e.g., gas-like diffusivity and liquid-like density). A diffuse interface method is commonly employed in supercritical and transcritical jet simulations to capture the properties of the flow [2]–[4]. Several difficulties should be overcome for simulating the mixing of the jets using a diffused interface [5]. The presence of large density gradients between the liquid-like and the gas-like regions, the need of using a real-fluid EoS, or the spurious pressure oscillations generated in conservative schemes are the main challenges.

High order reconstruction methods are usually applied to capture the large density gradients. The authors of [6] performed a two-dimensional large-eddy simulation (LES) of supercritical mixing and combustion employing a fourth-order flux-differencing scheme and a total-variation-diminishing (TVD) scheme in the spatial discretization. In [7] a fourth-order central differencing scheme with fourth-order scalar dissipation was applied in order to stabilize the simulation of a cryogenic fluid injection and mixing under supercritical conditions. Moreover, [8] employed an eighth-order finite differencing scheme to simulate homogeneous isotropic turbulence under supercritical pressure conditions, while in [9] a density-based sensor was utilized, which switches between a second-order ENO (Essentially non-oscillatory) and a first-order scheme to suppress oscillations. In the present study a fifth-order WENO (Weighted Essentially Non-Oscillatory) scheme [10] is applied due to its high order accuracy and non-oscillatory behaviour.

Cubic EoS models like PR (Peng-Robinson) [11] and SRK (Soave-Redlich-Kwong) EoS [12] are usually used in supercritical and transcritical simulations. In the studies reported in [4], [13]–[15] the SRK EoS was employed in order to close the Navier Stokes equations and compute the fluid properties under supercritical and transcritical conditions. Moreover, the works reported in [3], [9], [16], [17] modeled the non-ideal fluid behavior applying the PR EoS. However, cubic models commonly present low accuracy computing the thermodynamic properties of hydrocarbons at temperatures typical for injection systems [2]. To overcome this, the Statistical Association Fluid Theory Equation of State (SAFT EoS) can be employed. This molecular model is based on the perturbation theory, as extensively studied in [18]–[21] by Wertheim. The authors of [22], [23] developed this EoS by applying Wertheim's theory and extending it to mixtures. Figure 1 shows a schematic representation of the terms considered in the SAFT equation. Each molecule is represented by segments of equal size, assumed to form a repulsive, hard sphere reference fluid. Next, the attractive interactions between segments are added to the model. The segment-segment energy needed to form a chain between the hard-sphere fluid segments is included and, if the segments exhibit associative interactions, such as hydrogen bonding, a term for this interaction is also added.

Among the different variants of the SAFT model, the PC-SAFT is the one implemented here. In this model, hard chains are used as the reference fluid instead of hard spheres. While the SAFT EoS computes segment-segment attractive interactions, the PC-SAFT EoS computes chain-chain interactions, which improves the thermodynamic description of chain-like, fluid mixtures [24].

Several papers have been published pointing out the advantages of the SAFT models with respect to the cubic EoS commonly used in CFD simulations. For example, [25] describes how the PC-SAFT model is better than cubic EoS for predicting gas phase compressibility factors and oil phase compressibilities. In [26] the superiority of the PC-SAFT performance is demonstrated relative to the Cubic Plus Association (CPA) EoS in correlating second order derivative properties, like speed of sound, dP/dV and dP/dT derivatives, heat capacities and the Joule–Thomson coefficient in the alkanes investigated. Similarly, [27] points out the superiority of the SAFT-BACK EoS over the PR EOS, particularly at high-density conditions, for computing second order derivative properties such as sound velocity and isobaric and isochoric properties. The study of [28] states that cubic EoS predict a linear increase of the Z factor (compressibility factor) with pressure, while the PC-SAFT EoS shows a better pressure dependence. Finally, [29] shows how the sPC-SAFT (simplified PC-SAFT) is more precise than SRK and CPA to compute the speed of sound of normal alkanes and methanol.

If a fully conservative (FC) formulation is employed along with a real-fluid EoS, spurious pressure oscillations may appear; the work of [4] has related this problem to computational stability issues, turbulence, and acoustics accuracy loss. The same authors of [4] developed a quasi-conservative (QC) scheme solving a pressure evolution equation instead of the energy conservation equation, while [30] developed a quasi-conservative framework where the artificial dissipation terms in the mass, momentum and energy equations are related and the pressure differential is considered to be zero. In [31] the double flux model was developed to avoid spurious pressure oscillations in simulations of compressible multicomponent flows that employ a perfect gas EoS; [32] extended it to reactive flows; and finally, [3], [17], [33] extended the double flux model to real-fluids and transcritical conditions. However, recently it has been reported that the large energy conservation error in quasi-conservative schemes maybe produce an unphysical quick heat-up of the jet [2].

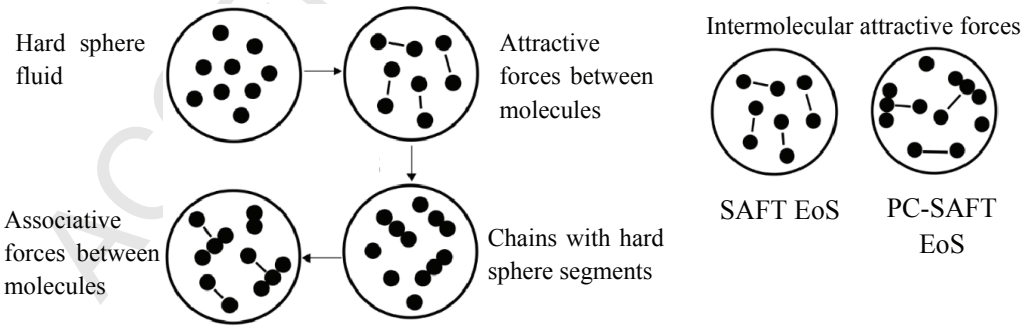

Figure 1. Schematic representation of the attractive and repulsive contributions of the SAFT EoS and the PC-SAFT EoS [24]

The novelty of the approach described here is the coupling of the PC-SAFT EoS with the Navier-Stokes equations, which it is not present in the literature. During the last years conservative and quasi-conservative formulations have been employed in the simulation of

supercritical and transcritical jets. For this reason, two codes have been developed employing both schemes: the conservative and the so-called quasi-conservative approach, where the double flux model of [3], [17], [33] is utilized**.** The aim of this research is not to solve the spurious pressure oscillations characteristic of FC schemes when real-fluid EoS are applied or the energy conservation error of QC formulations but to present how the Navier-Stokes equations can be closed with the PC-SAFT in both scenarios. Advection test cases and shock tube problems are included to show the overall performance of the developed framework using both formulations. Moreover, two-dimensional simulations of nitrogen and dodecane jets are presented to demonstrate the capability of the code to predict fluid mixing.

2. Numerical Method

The Navier-Stokes equations for a non-reacting multi-component mixture containing N species in a x-y 2D Cartesian system are given by:

$$\frac{\partial \mathbf{U}}{\partial t}+\frac{\partial \mathbf{F}}{\partial x}+\frac{\partial \mathbf{G}}{\partial y}=\frac{\partial \mathbf{F}_v}{\partial x}+\frac{\partial \mathbf{G}_v}{\partial y} \tag{1}$$

The vectors of eq. 1 are:

$$\mathbf{U}=\begin{bmatrix}\rho Y_1\\ \vdots\\ \rho Y_N\\ \rho u\\ \rho v\\ \rho E\end{bmatrix},\ \mathbf{F}=\begin{bmatrix}\rho u Y_1\\ \vdots\\ \rho u Y_N\\ \rho u^2+p\\ \rho uv\\ (\rho E+p)u\end{bmatrix},\ \mathbf{G}=\begin{bmatrix}\rho v Y_1\\ \vdots\\ \rho v Y_N\\ \rho vu\\ \rho v^2+p\\ (\rho E+p)v\end{bmatrix},\ \mathbf{F}_v=\begin{bmatrix}J_{x,1}\\ \vdots\\ J_{x,N}\\ \sigma_{xx}\\ \sigma_{xy}\\ u\sigma_{xx}+v\sigma_{xy}-q_x\end{bmatrix},\tag{2}$$

$$\mathbf{G}_v=\begin{bmatrix}J_{y,1}\\ \vdots\\ J_{y,N}\\ \sigma_{yx}\\ \sigma_{yy}\\ u\sigma_{yx}+v\sigma_{yy}-q_y\end{bmatrix}$$

where ρ is the fluid density, u and v are the velocity components, p is the pressure, E is the total energy, J_i is the mass diffusion flux of species i, σ is the deviatoric stress tensor and q is the diffusion heat flux vector.

The finite volume method has been applied in this work for obtaining a numerical solution to the above equations. The PC-SAFT EoS is implemented to simulate supercritical and transcritical states. The developed numerical framework considers a condition of thermodynamic equilibrium in each cell. Phase separations or metastable thermodynamic states are beyond the scope of this research and are not considered.

2.1 Formulations

Since PC-SAFT EoS is rarely used in CFD simulations, two codes have been developed employing different formulations (conservative and quasi-conservative) to

determine which one is more appropriate for the simulation of transcritical and supercritical fluid jets.

2.1.1 Conservative formulation

Operator splitting [34] is adopted to divide the physical processes into hyperbolic and parabolic sub-steps. The global time step is computed using the CFL (Courant–Friedrichs–Lewy) criterion of the hyperbolic operator.

Hyperbolic sub-step

The HLLC (Harten-Lax-van Leer-Contact) solver is used to solve the Riemann problem. The conservative variables are interpolated onto the cell faces using a fifth-order WENO scheme [10] due to its high order accuracy and non-oscillatory behaviour. TVD (Total Variation Diminishing) limiters [34] are applied to avoid oscillations near discontinuities. Time integration is performed using a SSP-RK3 (third-order strong-stability-preserving Runge–Kutta) method [35].

Parabolic sub-step

The method developed in [36] is applied to calculate the values of the dynamic viscosity and thermal conductivity of the mixture. The model of [37] is implemented to compute the diffusion coefficient. A RK2 (second-order Runge–Kutta) scheme is employed to perform the time integration of this sub-step. Linear interpolation is performed for computing the conservative variables, enthalpy and temperature on faces from cell centres.

2.1.2 Quasi-conservative formulation

The physical processes are divided into hyperbolic and parabolic sub-steps using operator splitting as well [34]. The CFL criterion of the hyperbolic operator is used to compute the global time step.

Hyperbolic sub-step

The double flux model of [3], [17], [33] has been implemented. The HLLC solver is used to solve the Riemann problem. In the one-dimensional cases presented, the primitive variables are interpolated onto the cell faces using a fifth-order WENO scheme [10]. In the two-dimensional cases, a sensor that compares the value of the density in the faces and the centre of the cells is employed to determine in which regions a more dissipative scheme must be applied [3] . If the sensor is activated, TVD limiters [34] are employed. The solution is then blended with a first-order scheme (90% WENO). Time integration is performed using a SSP-RK3 method [35].

The following steps were followed to implement the double flux model [3], [17], [33]:

1) In each cell are stored the values of γ^* (eq.3) and e_0^* (eq.4).

$$\gamma^* = \frac{\rho c^2}{p} \tag{3}$$

$$e_0^* = e - \frac{pv}{\gamma^* - 1} \tag{4}$$

where p is the pressure, c is the sound speed, e is the internal energy and v is the specific volume.

2) Runge-Kutta scheme

- Step 1: The fluxes at the faces are computed using the primitive variables. The total energy in the left (L) and right (R) states are computed using eq.5.

$$(\rho E)^n_{L,R} = \frac{p^n_{L,R}}{\gamma^{*,n}_j - 1} + \rho^n_{L,R} e^{*,n}_{0,j} + \frac{1}{2}\rho^n_{L,R}\mathbf{u}^n_{L,R}\cdot\mathbf{u}^n_{L,R} \quad (5)$$

- Step 2: Update conservative variables using the RK scheme
- Step 3: Update primitive variables (using the double flux model to compute the pressure).

3) Update total energy**:** The total energy is updated from primitive variables based on the EoS (eq.6). Only at this point the PC-SAFT EoS is used to compute the internal energy, sound speed, temperature and enthalpy.

$$\rho E = \rho e + \frac{1}{2}\rho\mathbf{u}\cdot\mathbf{u} \quad (6)$$

Parabolic sub-step

The diffusion fluxes are calculated conservatively in the same way that is explained in the conservative formulation.

2.2 PC-SAFT EoS subroutine

A different subroutine has been developed for each formulation because of the different inputs of the EoS subroutine.

Conservative formulation

The thermodynamic variables computed in the CFD code by the PC-SAFT EoS are the temperature, pressure, sound speed and enthalpy. The algorithm inputs are the density, internal energy, molar fractions and three pure component parameters per component (number of segments per chain, energy parameter of each component and segment diameter), see Table 1. The density and the internal energy are obtained from the conservative variables of the CFD code. The molar fractions are computed using the mass fractions employed in the continuity equations and the molar weights of the components. The pure component parameters are specified in the initialization of the simulation. A detailed description of the PC-SAFT EoS can be found in the Appendix A.

The Newton-Raphson method is employed to compute the temperature that is needed to calculate the value of all other thermodynamic variables. The temperature dependent function used in the iterative method is the internal energy. Initially, a temperature value is assumed (for example the value of the temperature from the previous time RK sub-step or from the previous time step) to initialize the iteration process. In most cells, this value is close to the solution. Then the compressibility factor is calculated as the sum of the ideal gas contribution (considered to be 1), the dispersion contribution and the residual hard-chain contribution (Appendix A):

$$Z = 1 + Z^{hc} + Z^{disp} \quad (7)$$

The pressure is then calculated using eq.8 once the compressibility factor is known [38]:

$$p = Z k_B T \rho_m \left(10^{10}\right)^3 \tag{8}$$

where k is the Boltzmann constant and ρ_m is the total number density of molecules.

Finally, the internal energy is estimated as the sum of the ideal internal energy and the residual internal energy. The ideal internal energy is computed using the ideal enthalpy. The residual internal energy is calculated using eq.9 [39]:

$$\frac{e^{res}}{RT} = -T\left(\frac{\partial \tilde{a}^{res}}{\partial T}\right)_{\rho, x_i} \tag{9}$$

where $\tilde{a}^{res}$ is the reduced Helmholtz free energy.

If the difference between the internal energy computed with the PC-SAFT model and the value obtained from the conservative variables is bigger than 0.001J/kg, the Newton-Raphson method is applied to calculate a new value of the temperature and the aforementioned steps are repeated, see Appendix D.

Quasi-conservative formulation

The thermodynamic variables computed in the CFD code by the PC-SAFT EoS are the temperature, internal energy, sound speed and enthalpy. The algorithm inputs are the density, pressure, molar fractions and three pure component parameters per component. The density and mass fractions (used to compute the molar fractions) are obtained from the conservative variables. The pressure is obtained employing the double flux model. The temperature is iterated until the difference between the pressure computed with the PC-SAFT model and the value obtained from the double flux model is lower than 0.001Pa, see Appendix D.

2.3 Peng-Robinson EoS and PC-SAFT EoS comparison

The most attractive feature of the PC-SAFT EoS is the better prediction of derivative properties such as compressibility and speed of sound. [27] shows the inaccuracy of cubic models to predict second derivative properties such as isobaric heat capacity and sound velocity in hydrocarbons at high density ranges. In the case of the sonic fluid velocity, the AAD% (Average Absolute Deviation) by PR EoS for methane, ethane, and propane are 28.6%, 14.7%, and 61.2%, respectively.

Figure 2 presents a comparison of the thermodynamic properties of n-dodecane at 6MPa computed using the PC-SAFT EoS and the Peng-Robinson EoS. NIST Refprop [40] has been used as reference due to its extensive validation with experimental data. While the results of both EoS are quite similar at density values lower than 550 Kg/m^3 there is a significant difference at higher densities, especially in the sound speed. Cubic models commonly present low accuracy computing the thermodynamic properties of hydrocarbons at temperatures typical for injection systems [2]. However, the PC-SAFT EoS shows an accuracy similar to NIST without the need of an extensive model calibration as only three parameters are needed to model a specific component. Another advantage is the possibility of computing the thermodynamic properties of mixtures; NIST has limited mixture combinations.

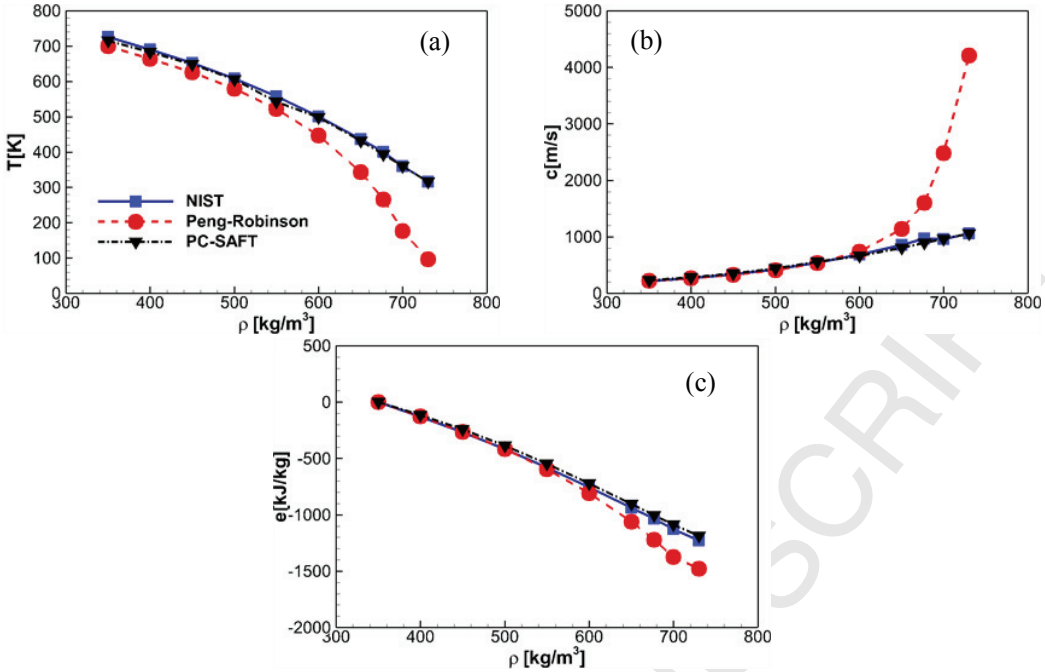

Figure 2: Comparison of thermodynamic properties of n-dodecane at 6MPa computed using the PC-SAFT EoS and the Peng-Robinson EoS: (a) density, (b) sound speed, (c) internal energy

3. Results

Initially, advection test cases and shock tube problems are solved to validate the hyperbolic part of the numerical framework employing the conservative and quasi-conservative formulations, while the parabolic part is omitted. Following, two-dimensional simulations of transcritical and supercritical nitrogen and dodecane jets are presented, including the parabolic part, to prove the multi-dimensional capability of the code.

3.1. One-dimensional cases

3.1.1 Advection test cases

Conservative formulation

Figure 3 shows the results of the supercritical Advection Test Case 1, see Table 2. Nitrogen is used as working fluid (The critical properties of nitrogen are $p_{c,N2}$ = 3.4 MPa and $T_{c,N2}$ = 126.2 K). The computational domain is x ϵ [0, 1] m; the initial conditions in 0.25m < x < 0.75m are ρ=250 kg/m^3, p=5 MPa, and T=139.4 K; in the rest of the domain are ρ= 45.5 kg/m^3, p=5 MPa, and T=367.4 K. The advection velocity applied is 50m/s; periodic boundary conditions are utilized; a uniform grid spacing of 0.01m is employed; the simulated time is t=0.02s; and the CFL is set to be 0.5. Four spatial discretization schemes are compared: fifth-order WENO, second-order (based on the Minmod limiter), first order and a blend of the fifth-order WENO and the first-order schemes (95% WENO and rest 1st order).

The oscillations are more severe when high-order reconstruction schemes are applied. By blending a high-order scheme and a low-order model, dissipation can be used to smooth the numerical solution. If the advection test case is initialized using a smooth profile no spurious pressure oscillation appear in the solution as the sharp jumps in the thermodynamic properties between cells are avoided, see Figure 4. The smooth initial interface was generated as described in [13] using eq.10.

$$q = q_L(1 - f_{sm}) + q_R f_{sm} \tag{10}$$

$$f_{sm} = \frac{(1 + erf[\Delta R / \varepsilon])}{2} \tag{11}$$

Where L and R refers to the left and right states respectively and ΔR is the distance from the initial interface. $\varepsilon = C_\varepsilon \Delta x$, where Δx is the grid spacing and C_ε is a free parameter to determine the interface smoothness set to be 8.

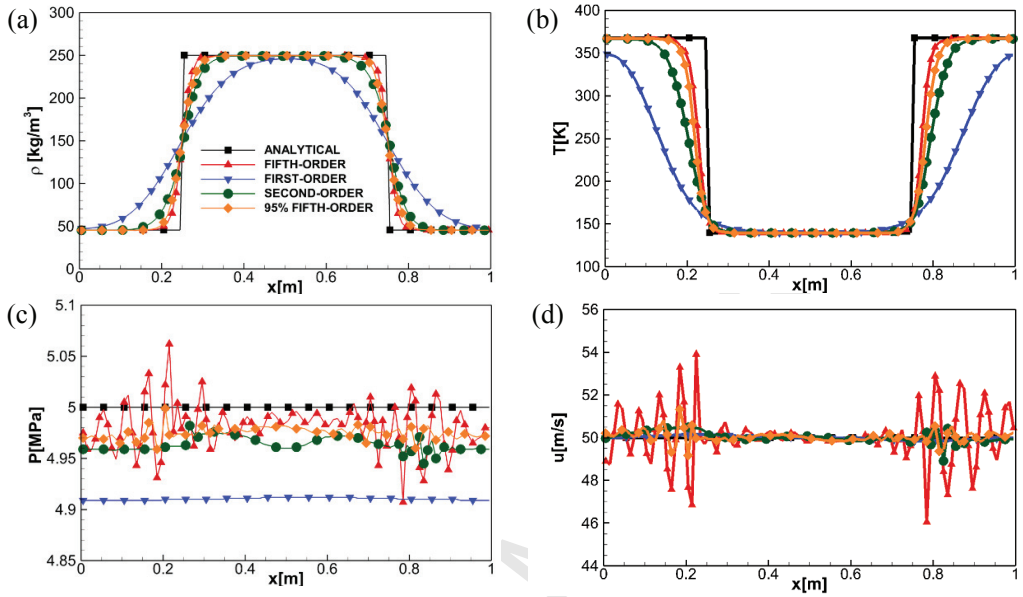

Figure 3. Advection Test Case 1 (N_2), FC formulation, CFL = 0.5, u = 50 m/s, 100 cells, t=0.02 s. Comparison of the (a) density, (b) temperature, (c) pressure and (d) x-velocity between the analytical and the numerical solution.

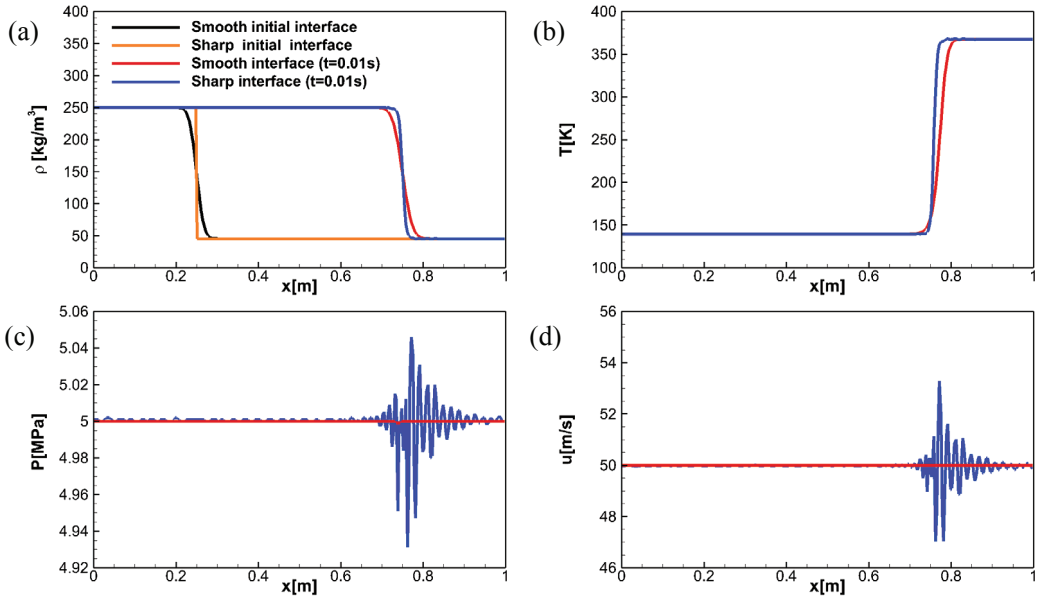

Figure 4. Advection Test Case 1 (N_2), FC formulation, CFL = 0.5, u = 50 m/s, 300 cells, t=0.01 s. Comparison of the (a) density, (b) temperature, (c) pressure and (d) x-velocity between the analytical and the numerical solution.

Quasi-conservative formulation

Figure 5 presents the results of the transcritical Advection Test Case 1 solved using the QC formulation. The advection velocity applied is 50m/s; periodic boundary conditions are applied; a uniform grid spacing of 0.01m is used; the simulated time is t=0.02s; and the CFL is set to be 1. Unlike the fully conservative scheme, spurious pressure oscillations are not present in the solution.

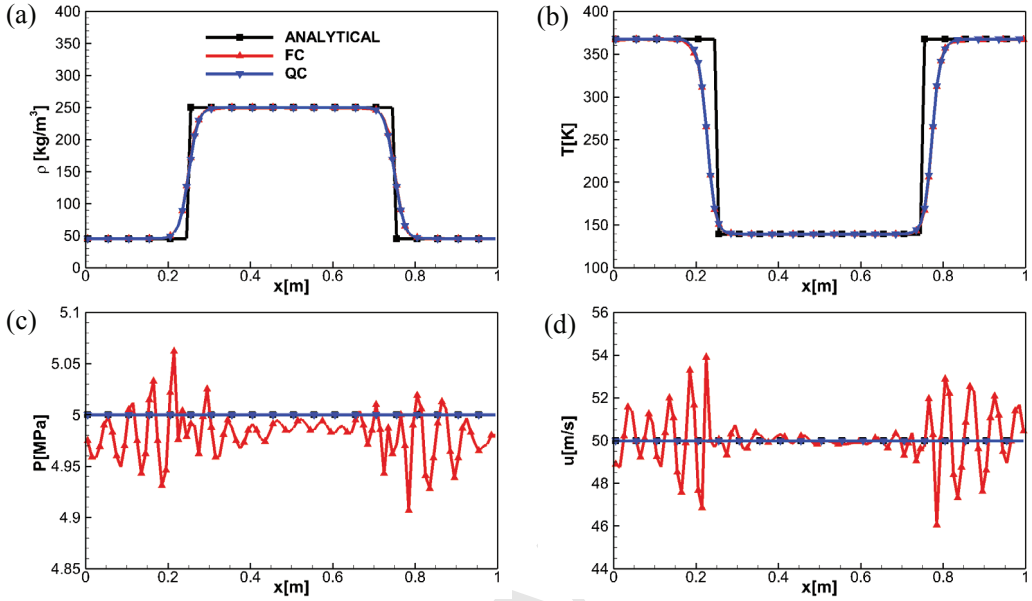

Figure 5. Advection Test Case 1 (N_2), FC and QC formulations, CFL(FC) = 0.5, CFL(QC)=1.0, u = 50 m/s, 100 cells, t=0.02 s. Comparison of the (a) density, (b) temperature, (c) pressure and (d) x-velocity between the analytical and the numerical solution.

Figure 6 presents the results of the transcritical Advection Test Case 2 where nitrogen is used as working fluid, see Table 2. The computational domain is x ϵ [0, 1] m; the initial conditions in 0.25 m < x < 0.75 m are ρ=804.0 kg/m^3, p=4 MPa, and T=84.41 K; in the rest of the domain the initial conditions are ρ=45.5 kg/m^3, p=4 MPa, and T=299.0 K. The advection velocity utilized is 100 m/s; periodic boundary conditions are used; the computational domain is x ϵ [0, 1] m; 150 cells are employed; the simulated time is t=0.01 s; a fifth-order WENO discretization scheme is used; and the CFL is set to be 1.0. It can be observed how large density gradients are solved without spurious pressure oscillations applying the double flux model.

Figure 7 shows the results of the transcritical advection of n-dodecane at supercritical pressure and subcritical temperature ($p_{c,n\text{-dodecane}}$ =1.817 MPa, $T_{c,n\text{-dodecane}}$ =658.1 K) in supercritical nitrogen, Advection Test Case 3 (Table 2). The computational domain is x ϵ [0,1] m; the initial conditions in 0.25m < x < 0.75m are $\rho_{n\text{-dodecane}}$ =700.0 kg/m^3, $p_{n\text{-dodecane}}$ = 6MPa, and $T_{n\text{-dodecane}}$ =360.1 K; in the rest of the domain ρ_{N2} =20.0 kg/m^3, p_{N2} =6 MPa, and T_{N2} =965.7 K. The advection velocity utilized is 100 m/s; periodic boundary conditions are used; 150 cells are employed; the simulated time is t=0.01 s; a fifth-order WENO discretization scheme is used; and the CFL is set to be 1.0. Unlike conservative codes, velocity and pressure equilibriums are preserved in multicomponent cases if the double flux model is applied.

404 **Table 1. PC-SAFT pure component parameters [38]**

	m	$\sigma[\text{Å}]$	$\varepsilon/\text{k}[\text{K}]$
NITROGEN	1.2053	3.3130	90.96
DODECANE	5.3060	3.8959	249.21

405
406
407 **Table 2. 1D Test Cases**

ADVECTION TEST CASES			
CASE 1	Pressure [MPa]	Density [kg/m^3]	Temperature [K]
0.25 m < x < 0.75 m	N_2, 5	N_2, 250	N_2, 139.4
0.25 m > x or x > 0.75 m	N_2, 5	N_2, 45.5	N_2, 367.4
CASE 2			
0.25 m < x < 0.75 m	N_2, 4	N_2, 804	N_2, 84.4
0.25 m > x or x > 0.75 m	N_2, 4	N_2, 45.5	N_2, 299.0
CASE 3			
0.25 m < x < 0.75 m	n-dodecane, 6.0	n-dodecane, 700.0	n-dodecane, 360.1
0.25 m > x or x > 0.75 m	N_2, 6.0	N_2, 20.0	N_2, 965.7
SHOCK TUBE PROBLEM			
PROBLEM	Pressure [MPa]	Density [kg/m^3]	Temperature [K]
x < 0.5 m	n-dodecane, 13.0	n-dodecane, 700.0	n-dodecane, 372.8
x > 0.5 m	n-dodecane, 6.0	n-dodecane, 150.0	n-dodecane, 944.4

408
409
410 **Table 3. 2D Test Cases**

CASE A	Pressure [MPa]	Density [kg/m^3]	Temperature [K]
JET	N_2, 4.0	N_2, 804.0	N_2, 84.4
CHAMBER	N_2, 4.0	N_2, 45.5	N_2, 299.5
CASE B			
JET	N_2, 4.0	N_2, 440.0	N_2, 127.0
CHAMBER	N_2, 4.0	N_2, 44.5	N_2, 305.0
CASE C			
JET	n-dodecane, 11.1	n-dodecane, 450.0	n-dodecane, 687.2
CHAMBER	N_2, 11.1	N_2, 37.0	N_2, 972.9

411

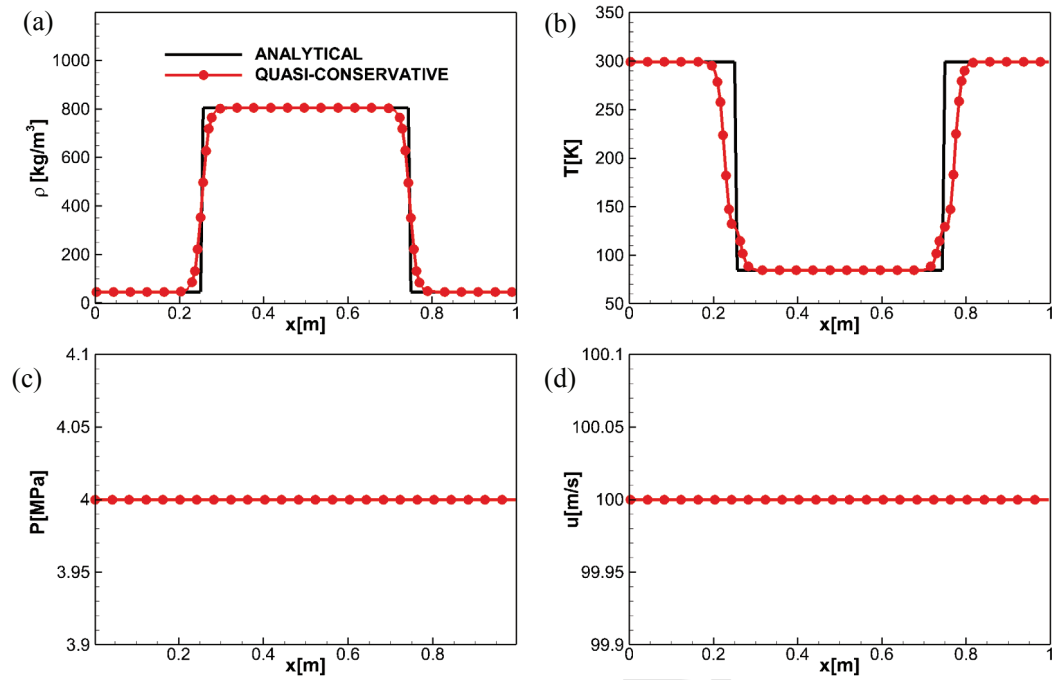

Figure 6. Advection Test Case 2 (N_2), QC formulations, CFL = 1.0, u = 150 m/s, 100 cells, t=0.01s. Comparison of the (a) density, (b) temperature, (c) pressure and (d) x-velocity between the analytical and the numerical solution.

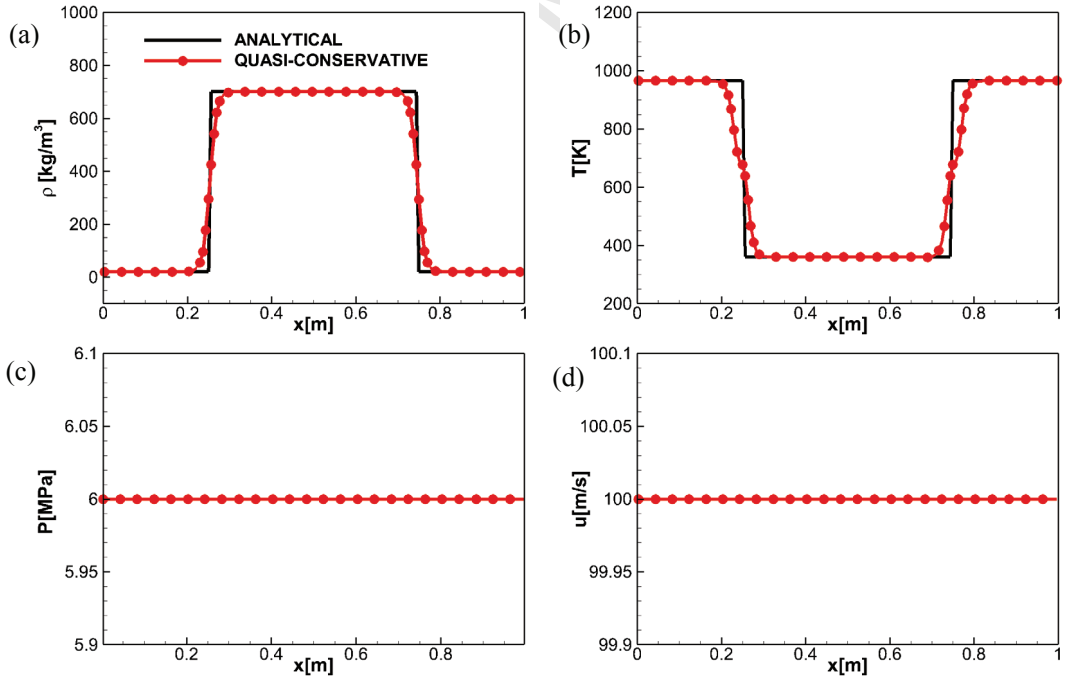

Figure 7. Advection Test Case 3 (N_2 - Dodecane), QC formulations, CFL = 1.0, u = 100 m/s, 150 cells, t=0.01 s. Comparison of the (a) density, (b) temperature, (c) pressure and (d) x-velocity between the analytical and the numerical solution.

Energy conservation error in the quasi-conservative formulation

The evolution of the energy conservation error of the Advection Test Case 2 is presented in Figure 8 . The error has been evaluated employing eq.12 [3].

$$\varepsilon = \left| \frac{\int_\Omega \left[(\rho E)(t) - (\rho E)(0) \right] dx}{\int_\Omega (\rho E)(0) dx} \right| \tag{12}$$

where ε is the relative error of the total energy respect to initial conditions and Ω is the computational domain.

The energy conservation error is higher using the PC-SAFT EoS than Peng-Robinson EoS. This is related to the fact that the profiles of γ^* and e_0^* are smoother employing the cubic model. There are shaper jumps in the internal energy and speed of sound employing the PC-SAFT EoS, see Figure 10. The error in the conservation of the energy depends on the jumps in the variables $1/\left(\gamma^* - 1\right)$ and e^* [3]. A convergence of the error to 0 exists increasing the refinement.

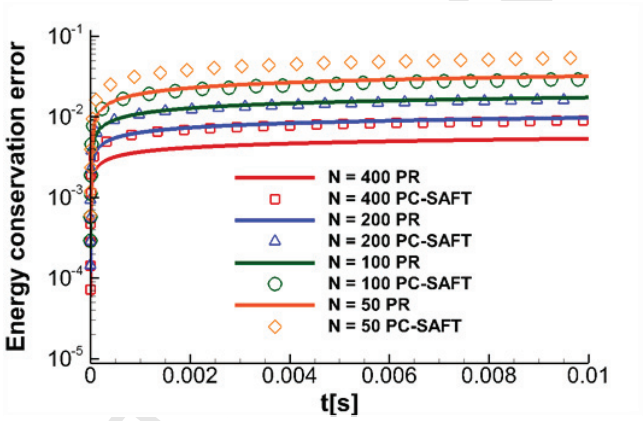

Figure 8. Relative energy conservation error computed using eq.10 of the QC formulation for the Advection Test Case 2 (Transcritical nitrogen) using the Peng-Robinson EoS (PR) and the PC-SAFT EoS. N is the number of cells employed.

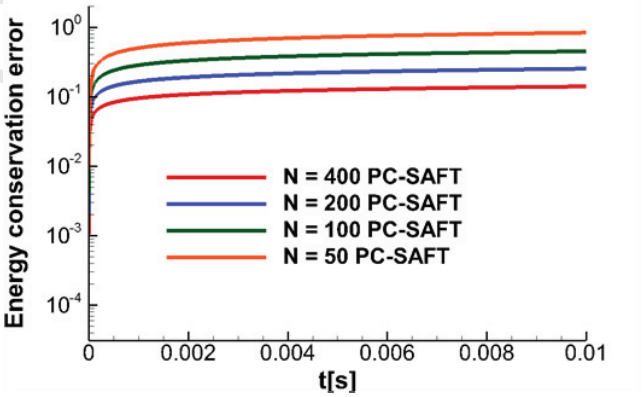

Figure 9. Relative energy conservation error computed using eq.10 of QC formulation for the Advection Test Case 3 using the PC-SAFT EoS. N is the number of cells employed.

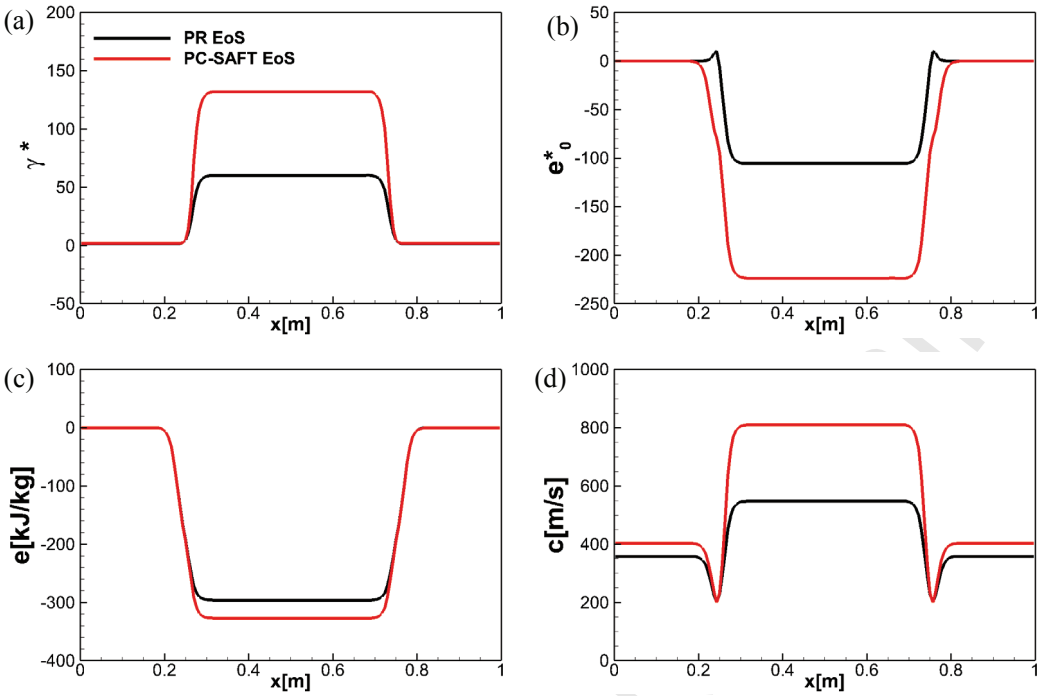

Figure 10. Advection Test Case 2 (N_2), QC formulation, CFL = 1.0, u = 150 m/s, 100 cells, t=0.01s. Comparison of γ* and e_0* computed using the Peng Robinson EoS (PR EoS) and the PC-SAFT in the Advection Test Case 2.

Figure 9 presents the evolution of the energy conservation error of the Advection Test Case 3. Because of the different thermodynamic properties of the components, a higher energy conservation error than in the single-species cases appears. Although, a convergence to 0 is observed in one-dimensional cases increasing the refinement like in the single-species cases.

3.1.2 Shock tube problems

The Euler equations are solved in this validation so a direct comparison with the exact solver can be done. The exact solution has been computed using the methodology described in [41].

Quasi-conservative formulation

The domain is x ϵ [0, 1] m. The working fluid employed is dodecane. A fifth-order WENO scheme is employed to interpolate the primitive variables onto the cell faces. 800 equally spaced cells were used. Wave transmissive boundary conditions are implemented in the left and right sides. The double flux model is applied. The pressure exceeds the critical value in all the domain while there is a transition in the temperature from subcritical to supercritical from left to right. The initial conditions in the left state are ρ_L=700 kg/m^3, p_L=13 MPa, u_L=0 m/s; and in the right state are ρ_R=150 kg/m^3, p_R=6 MPa, u_R=0 m/s. The simulated time is t=0.2 ms.

Figure 11 displays the results obtained for density, temperature, pressure and velocity. Despite being a quasi-conservative scheme, the double flux model [3], [17], [33] can solve strong shock waves in transcritical cases with a high degree of accuracy without generating spurious pressure oscillations.

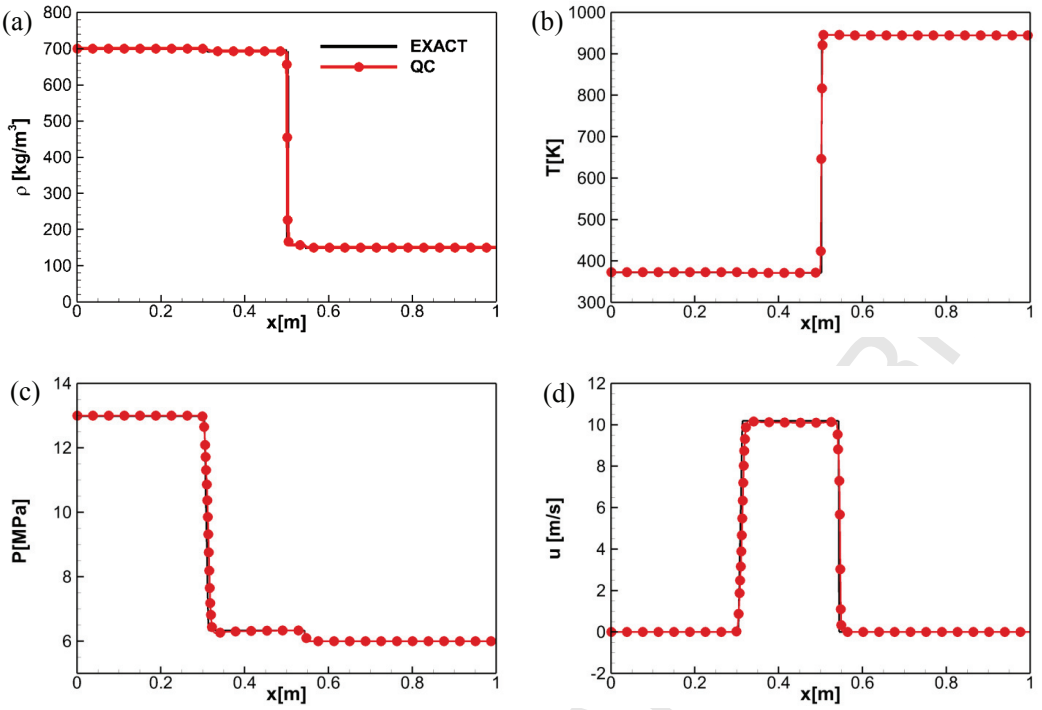

Figure 11. Shock Tube Problem 1 (Dodecane), QC formulation, CFL = 1.0, 800 cells, t=0.2 ms. Comparisons of (a) density, (b) temperature, (c) velocity and (d) pressure profiles: exact solution and numerical solution.

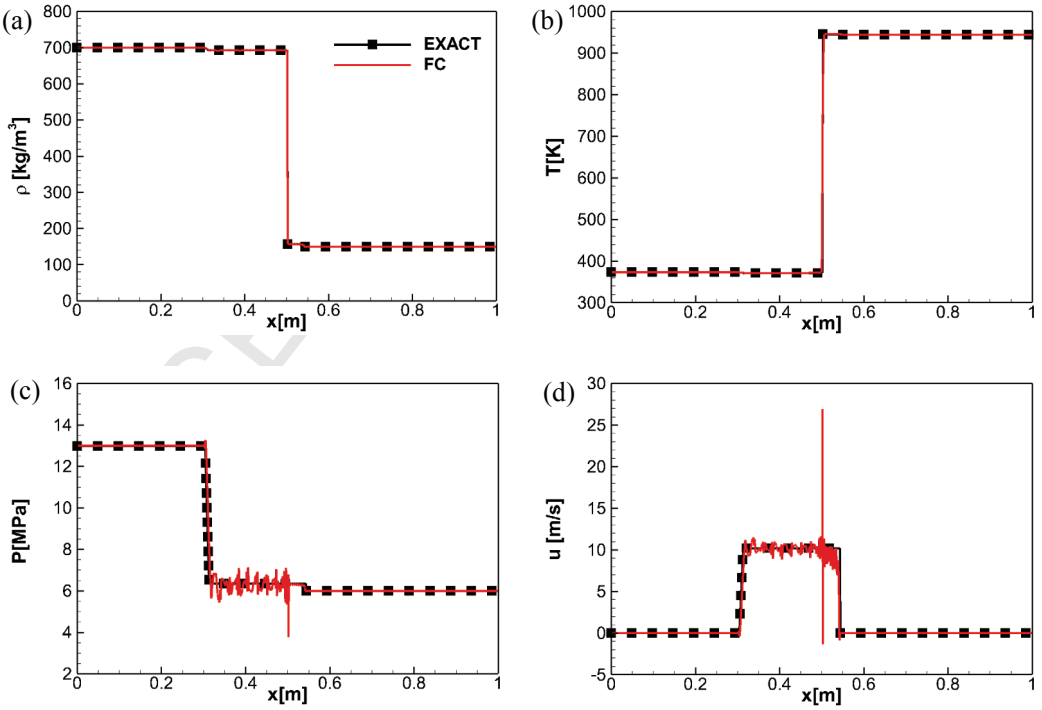

Figure 12. Shock Tube Problem 1 (Dodecane), FC formulation, CFL = 0.5, 4000 cells, t=0.2 ms. Comparisons of (a) density, (b) temperature, (c) velocity and (d) pressure profiles: exact solution and numerical solution.

Conservative formulation

The same shock tube problem described before is solved. A fifth-order WENO scheme is employed to interpolate the conservative variables onto the cell faces. Large spurious pressure oscillations appear in the solution because of the sharp jumps in the thermodynamic properties between cells, see Figure 12.

Comparison with the Peng-Robinson EoS (Quasi-conservative formulation)

Figure 13 shows the density, temperature, pressure, velocity, sound speed and internal energy of the same shock tube problem solved in a larger domain x ϵ [0, 2] m using the PC-SAFT and the Peng-Robinson EoS. The simulated time is t=0.3 ms. The quasi-conservative formulation has been employed. 800 equally spaced cells were used. A significant difference can be observed in the results between the two EoS. Due to the high deviation in the sound speed computed by the Peng-Robinson EoS in the high-density region, the expansion wave travels much faster using the cubic model. Moreover, the calculated temperatures are much lower using the Peng-Robinson EoS in the high-density region.

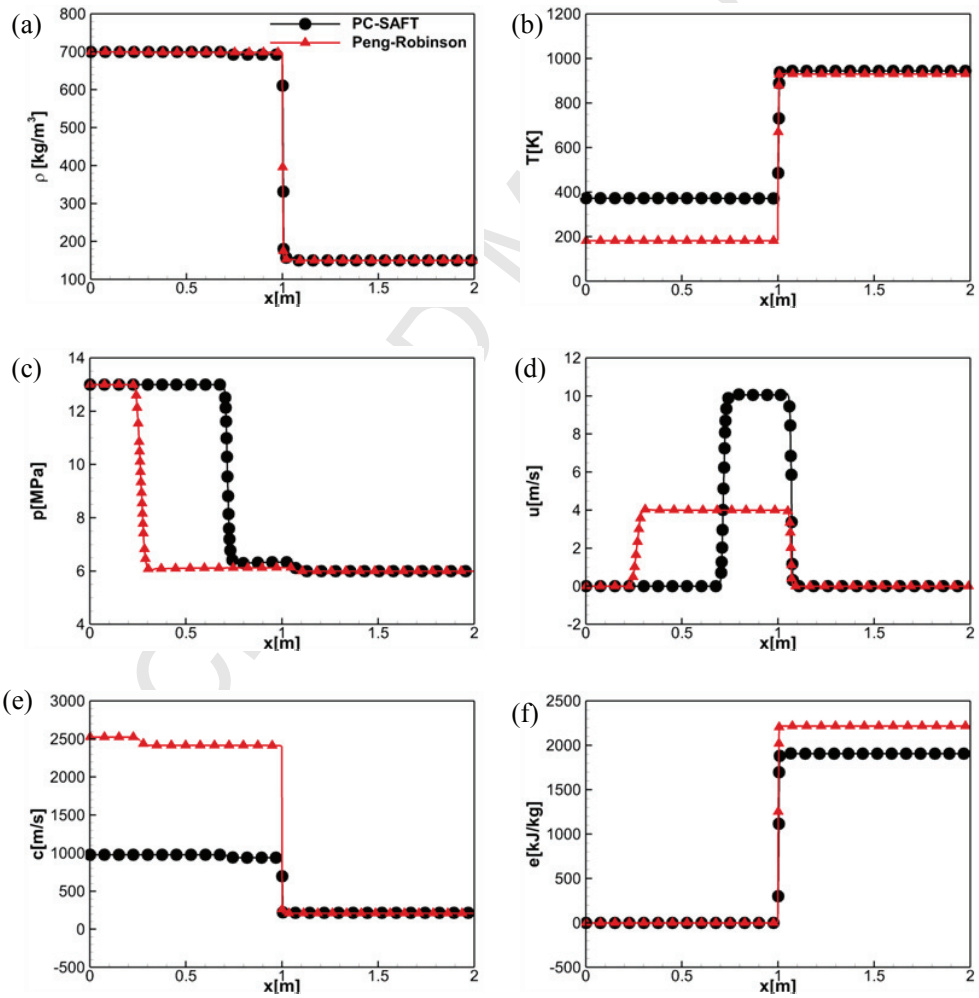

Figure 13. Shock Tube Problem 2 (Dodecane), QC formulation, CFL = 1.0, 800 cells, t=0.3 ms. Comparison of the (a) density, (b) temperature, (c) pressure, (d) x-velocity, (e) sound speed, (f) internal energy between the numerical solutions obtained using the Peng-Robinson EoS and the PC-SAFT EoS.

3.2 Two-dimensional cases

Planar two-dimensional simulations of transcritical and supercritical jets are presented in this section. The initial conditions are summarized in Table 3. The parabolic sub-step is included into these simulations, without sub-grid scale modelling for turbulence or heat/species diffusion.

Transcritical nitrogen injection (Quasi-Conservative formulation, Case A)

A structured mesh is applied with a uniform cell distribution. The cell size is 0.043 mm × 0.043 mm. The domain used is 30mm × 15mm. Transmissive boundary conditions are applied at the top, bottom and right boundaries while a wall condition is employed at the left boundary. A flat velocity profile is imposed at the inlet. The case is initialized using a pressure in the chamber of 4 MPa, the density of the nitrogen in the chamber is 45.5 kg/m^3 and the temperature is 299.5 K. The temperature of the jet is 84.4 K and the density is 804.0 kg/m. A summary of the initial conditions can be found in Table 3. The velocity of the jet is 100 m/s and the diameter of the exit nozzle is 1.0 mm.

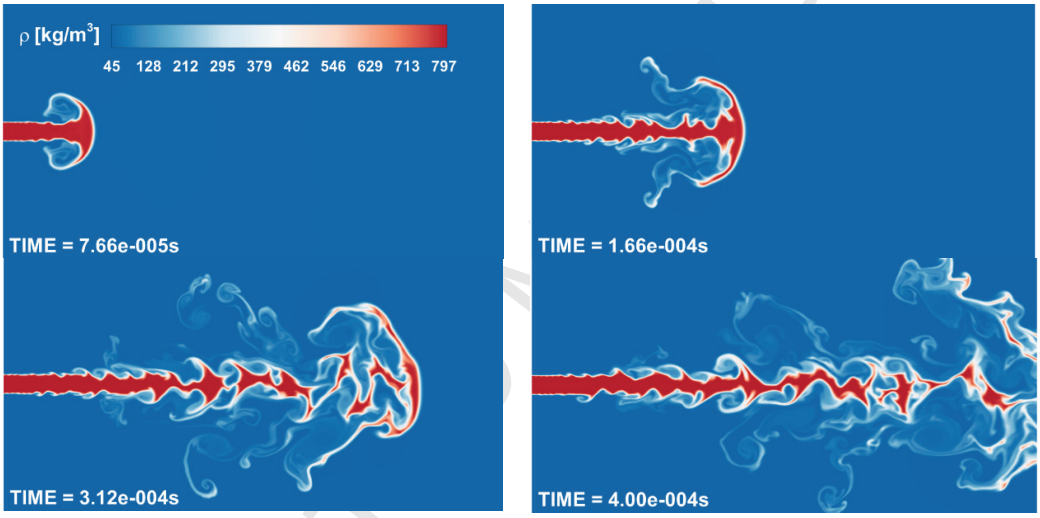

Figure 14. 2D Test Case A, CFL = 1.0, 245000 cells, QC formulation. Density results of the simulation of the planar cryogenic nitrogen jet at various times.

When the jet enters the elevated temperature environment of the chamber, the velocity gradients at the jet surface generate a vortex rollup that finally breakup into ligament-shaped structures, see Figure 14. The Kelvin Helmholtz instability can be observed in the shear layer, which is similar to a gas/gas turbulent mixing case. No droplets are formed at these conditions. The jet is quickly heated to a gas-like supercritical state after the injection takes place. It must be highlighted that the mesh resolution is not enough to resolve all the scales (the aim of these simulations is to test the developed numerical framework). Moreover, 2D simulation cannot resolve turbulence. Figure 17 shows the density, temperature, pressure and sound speed results at 4 x 10^{-4} s.

Figure 15 shows a scatter plot of pressure as a function of density for the planar cryogenic nitrogen jet. The simulated case remains in the hyperbolic region of the governing equations with a real-valued speed of sound (Appendix B). The mixing trajectory passes close to the critical point with a few individual points inside the saturation curve, which means that phase separation does not occur [42]. The larger fluctuations caused by the confined domain

or the two-dimensionality of the case could be the reason why a small number of cells are in the unstable region [3].

Although one of reasons of the prevailing usage of cubic EoS is their efficiency, practical simulations can be performed using the PC-SAFT EoS. The quasi-conservative formulation is computationally less expensive than the conservative scheme because the PC-SAFT EoS has to be used only once in the hyperbolic operator in each time step. The computational time is 65-70% higher using the PC-SAFT EoS than utilizing the PR EoS. Figure 16 shows the time taken by the code to solve the transcritical nitrogen injection case depending on the number of cells used (only one core is used to perform the simulation).

The PC-SAFT EoS is implemented using loops that depend on the number of components solved, which means that it takes more time to compute the properties of mixtures. However, knowing the mass fractions it is possible to determine how many components are present in a cell a priori. The PC-SAFT is then only solved for that specific number of components. Most cells along the simulation in the combustion chamber contain only nitrogen. For this reason, a significant increment on time has not been observed performing two-component simulations.

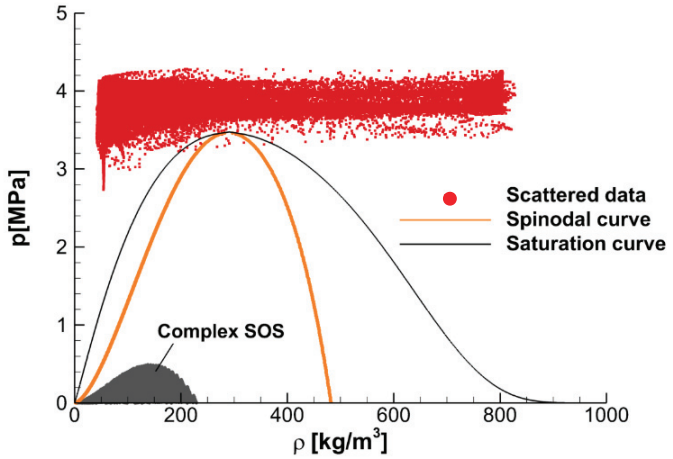

Figure 15. Scatter plot of pressure as a function of density for the transcritical nitrogen jet (Case A). The vapor dome, non-convex region and the region with complex speed of sound (SOS) are included.

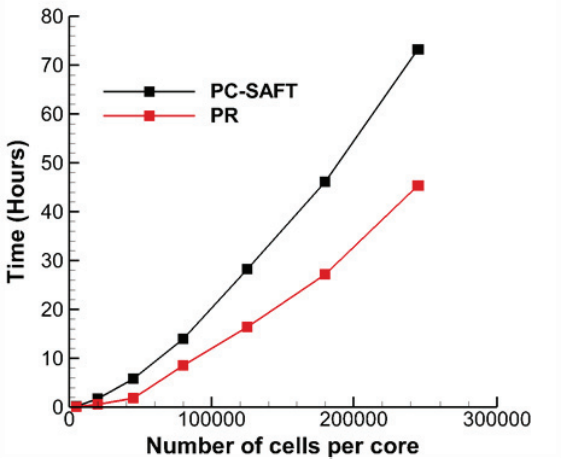

Figure 16. Computational time employed to compute the solution of the transcritical nitrogen jet (Case A) at t = 4 x 10^{-4} employing a variable number of cells.

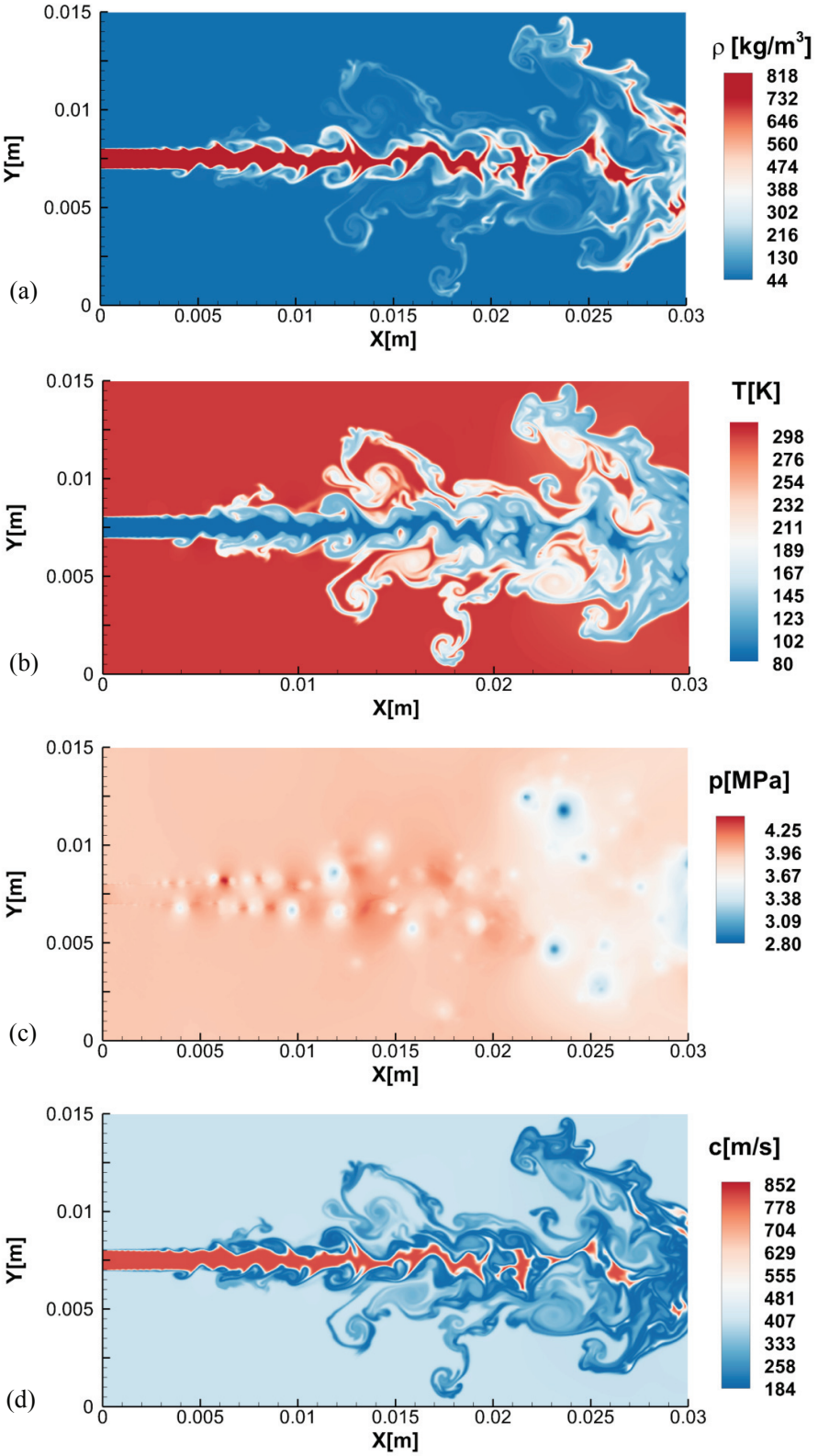

Figure 17. 2D Test Case A, CFL = 1.0, 245000 cells, QC formulation. Results of the simulation of the planar cryogenic nitrogen jet at t = 4 x 10^{-4} s using the quasi-conservative formulation: (a) density, (b) temperature, (c) pressure, (d) sound speed.

Supercritical nitrogen injection (Conservative formulation, Case B)

The case is initialized using a pressure in the chamber of 4 MPa, the density of the nitrogen in the chamber is 45.5 kg/m3 and the density of the jet is 440.0 kg/m^3 (Table 3). The velocity of the jet is 50 m/s. The spatial reconstruction is carried out using a blending of the fifth-order WENO and the first-order schemes (95% fifth-order WENO). The CFL number is set at 0.4. Transmissive boundary conditions are applied at the top, bottom and right boundaries while a wall condition is employed at the left boundary. A flat velocity profile is imposed at the inlet.

If sharp interface methods (i.e. front tracking method) are not applied, the interfaces are not sharp one-point jumps but smooth as they are resolved [43]. This is the reason why the wiggles that appear in this 2D simulation are not as severe as in the 1D cases presented in Section 3.1 initialized using a sharp interface, see Figure 18. The study of [43] shows how smooth interfaces can reduce the spurious pressure oscillations.

The minimum pressure encountered along the simulation is higher than the nitrogen critical pressure so there are no cells in the vapor-liquid equilibrium region. The heat-up of the jet follows the same density-temperature trajectory employing a FC or a QC formulation in single-species cases, see Figure 19. In the works of [2], [44] a different behaviour in multicomponent cases can be observed, where QC formulations follow an isobaric-isochoric mixing model for binary mixtures while conservative schemes follow an isobaric-adiabatic mixing model.

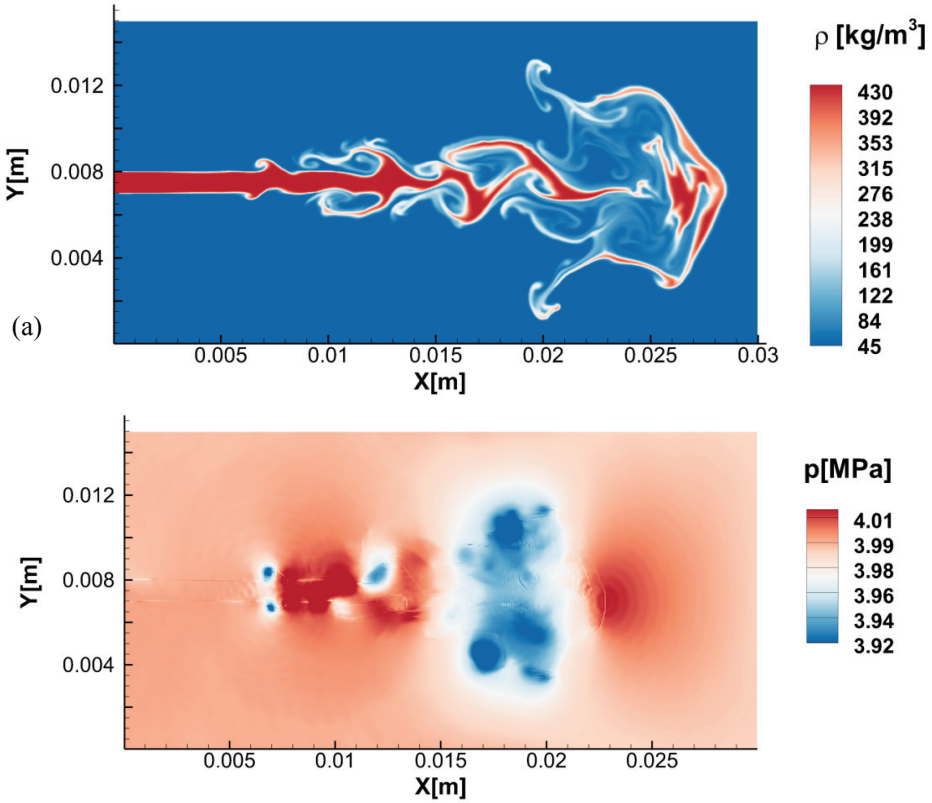

Figure 18. 2D Test Case B, CFL = 0.4, 180000 cells, FC formulation. Results of the simulation of the supercritical nitrogen jet at t = 7.84 x 10^{-4} s: (a) density, (b) pressure.

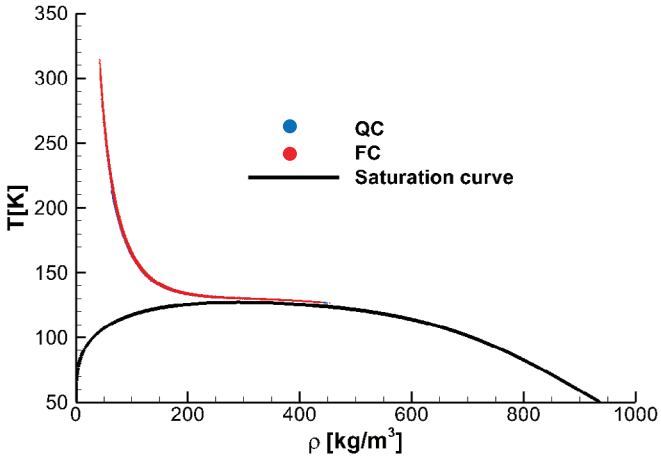

Figure 19. 2D Test Case B solved using the FC and QC formulations. Scattered data of density and temperature. The nitrogen vapor dome is included.

Supercritical dodecane injection (Conservative formulation, Case C)

Dodecane/nitrogen mixtures are Type IV as stated by [45], which means that the critical temperature of the mixture is an intermediate value of the critical temperature of both components and the mixture critical pressure is higher than the critical pressure of either component, see Figure 23. A simulation of a dodecane jet where VLE (Vapor-Liquid Equilibrium) conditions are avoided injecting the dodecane at a temperature higher than its critical value has been included to prove the multi-species capability of the code. To check that any cell is in a thermodynamic metastable state, the vapor-liquid saturation curves were computed (Appendix C).

A structured mesh is applied with a uniform cell distribution. The cell size is 8.3μm × 8.3μm. The domain used is 5mm × 2.5mm. Transmissive boundary conditions are applied at the top, bottom and right boundaries while a wall condition is employed at the left boundary. A flat velocity profile is imposed at the inlet. The case is initialized using a pressure in the chamber of 11.1 MPa, the density and the temperature of the nitrogen in the chamber are 37.0 kg/m^3 and 973 K (high-load Diesel operation conditions [46]) respectively. The density and temperature of the jet are 450.0 kg/m^3 and 687 K (Table 3). The velocity of the jet is 200 m/s and the diameter of the exit nozzle is 0.1 mm.

As in the transcritical nitrogen case ligament-shaped structures appear and the Kelvin Helmholtz instability can be observed in the shear layer, see Figure 20. The jet is quickly heated-up from a liquid-like supercritical state to a gas-like supercritical state. Some spurious oscillations appear in the pressure field because of the high non-linearity of the EoS. The quasi-conservative formulation was not employed because of the incorrect prediction of the jet heat-up that appear in multi-component cases [2], [44].

A comparison of averaged scattered data of composition and temperature and an isobaric-adiabatic mixing process can be seen in Figure 21. As [44] stated, fully conservative schemes describe an isobaric-adiabatic mixing process. The isobaric-adiabatic line in the Figure 21 was computed using eq.13-14 and the initial conditions of this case.

$$\dot{m}_3 = \dot{m}_1 + \dot{m}_2 \tag{13}$$

$$\dot{m}_3 h_3 = \dot{m}_1 h_1 + \dot{m}_2 h_2 \tag{14}$$

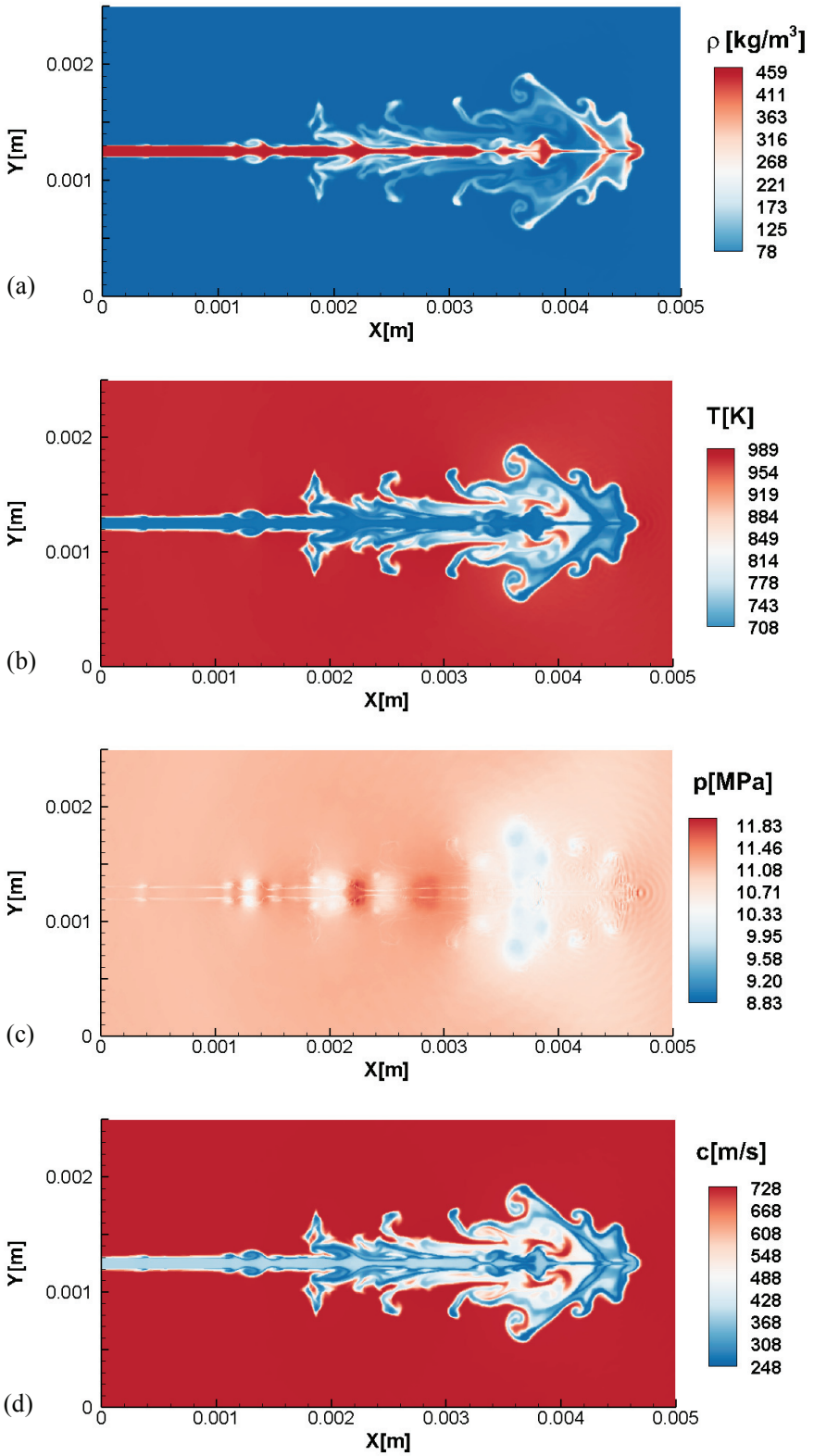

618 **Figure 20. 2D Test Case C, CFL = 0.5, 180000 cells, FC formulation. Results of the simulation of**
619 **the supercritical dodecane jet at t = 2.5 x 10^{-5} s: (a) density, (b) temperature, (c) pressure, (d)**
620 **sound speed.**
621

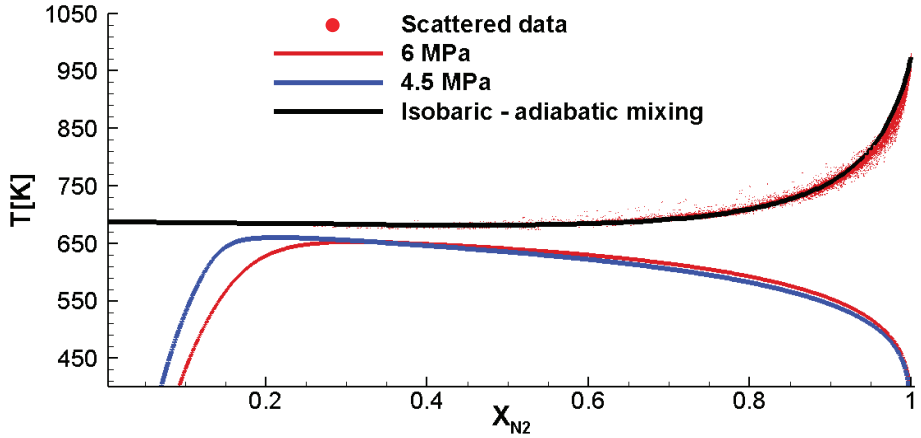

Figure 21. Scattered data of composition and temperature of the planar dodecane jet Case C. Solid lines are dodecane-nitrogen phase boundaries from VLE at 4.5 MPa and 6 MPa.

4. Conclusions

The Perturbated Chain Statistical Associating Fluid Theory (PC-SAFT) is utilized to close the Navier-Stokes equations using both a conservative and a quasi-conservative formulation, where the double flux model of [3], [17], [33] is applied. The PC-SAFT EoS presents a precision similar to NIST without the need of an extensive calibration as only three parameters are needed to model a specific component. It is presented as an alternative to the commonly used cubic EoS that present a low accuracy for computing the thermodynamic properties of hydrocarbons at temperatures typical for high pressure injection systems. Advection test cases and shock tube problems have been used to validate the hyperbolic operator of the developed numerical framework. The conservative formulation generates spurious pressure oscillations, like it has been reported with other diffuse interface density-based codes employing a real-fluid EoS. Due to fact that the interfaces are not sharp one-point jumps but smooth, as they are resolved in 2D simulations, the wiggles generated do not compromise the stability of the simulation. The quasi-conservative scheme can model transcritical single- and multicomponent cases without spurious pressure oscillations. Errors in the energy conservation that appear employing this formulation may produce an unphysical quick heat-up of the injected jet in multicomponent cases. Two-dimensional simulations of nitrogen and dodecane jets have been presented to demonstrate the multidimensional and multicomponent capability of the numerical framework.

Acknowledgments

This project has received funding from the European Union Horizon-2020 Research and Innovation Programme with grant Agreement No 675528.

Appendix A PC-SAFT EoS

The PC-SAFT EoS is expressed as the sum of all the residual Helmholtz free energy contributions. These contributions correspond to the distinct types of molecular interactions. The residual Helmholtz free energy is computed using eq.15 [38].

$$\tilde{a}^{res} = \tilde{a}^{hc} + \tilde{a}^{disp} \tag{15}$$

The hard-chain term, $\tilde{a}^{hc}$, for a mixture of nc components, is given in eq. 16

$$\tilde{a}^{hc} = \bar{m}\tilde{a}^{hs} - \sum_{i}^{nc} x_i (m_i - 1) \ln g_{ii}^{hs}(\sigma_{dii}) \tag{16}$$

where $\bar{m}$ is the number of segments for a multicomponent mixture (eq. 17), x_i is the mole fraction of every component i in the fluid, $\tilde{a}^{hs}$ is the hard sphere contribution (eq. 18), g_{ii}^{hs} is the radial distribution function of the hard-sphere fluid (eq.23) and m_i is the number of segments per chain of every component.

The number of segments for a multicomponent mixture is:

$$\bar{m} = \sum_{i}^{nc} x_i m_i \tag{17}$$

The hard sphere contribution is:

$$\tilde{a}^{hs} = \frac{1}{\varsigma_0}\left[\frac{3\varsigma_1\varsigma_2}{(1-\varsigma_3)} + \frac{\varsigma_2^3}{\varsigma_3(1-\varsigma_3)^2} + \left(\frac{\varsigma_2^3}{\varsigma_3^2} - \varsigma_0\right)\ln(1-\varsigma_3)\right] \tag{18}$$

ς_n is defined as:

$$\varsigma_n = \frac{\pi}{6}\rho_m \sum_i x_i m_i d_i^n \qquad n \in \{0,1,2,3\} \tag{19}$$

where ρ_m is the molecular density and d_i is the temperature-dependent segment diameter of component i (eq.21).

$$\rho_m = \frac{6}{\pi}\eta\left(\sum_i x_i m_i d_i^3\right)^{-1} \text{ being } \eta = \varsigma_3 \tag{20}$$

$$d_i = \sigma_{di}\left[1 - 0.12\exp\left(-3\frac{\varepsilon_i}{kT}\right)\right] \tag{21}$$

where k is the Boltzmann constant, T is the temperature and ε_i is the depth of pair potential of the component.

The mixture parameters σ_{ij} and ε_{ij} which are defined for every pair of unlike segments are modeled using a Berthelot-Lorentz combining rule.

$$\sigma_{ij} = \frac{1}{2}(\sigma_i + \sigma_j) \tag{22}$$

$$\varepsilon_{ij} = \sqrt{\varepsilon_i \varepsilon_j}(1 - k_{ij}) \tag{23}$$

where k_{ij} is the binary interaction parameter.

The radial distribution function of the hard-sphere fluid is:

$$g_{ij}^{hs} = \frac{1}{(1-\varsigma_3)} + \left(\frac{d_i d_j}{d_i + d_j}\right)\frac{3\varsigma_2}{(1-\varsigma_3)^2} + \left(\frac{d_i d_j}{d_i + d_j}\right)^2 \frac{3\varsigma_2^2}{(1-\varsigma_3)^3} \tag{24}$$

The dispersion term is defined as:

$$\tilde{a}^{disp} = -2\pi\rho_m I_1(\eta,\bar{m})\overline{m^2\varepsilon\sigma_d^3} - \pi\rho_m \bar{m} C_1 I_2(\eta,\bar{m})\overline{m^2\varepsilon^2\sigma_d^3} \tag{25}$$

where $\eta = \zeta_3$ is the reduced density, I_1 and I_2 are integrals approximated by simple power series in density

$$I_1(\eta,\bar{m}) = \sum_{i=0}^{6} a_i(\bar{m})\eta^i \tag{26}$$

$$I_2(\eta,\bar{m}) = \sum_{i=0}^{6} b_i(\bar{m})\eta^i \tag{27}$$

The coefficients a_i and b_i depend on the chain length:

$$a_i(\bar{m}) = a_{0i} + \frac{\bar{m}-1}{\bar{m}}a_{1i} + \frac{\bar{m}-1}{\bar{m}}\frac{\bar{m}-2}{\bar{m}}a_{2i} \tag{28}$$

$$b_i(\bar{m}) = b_{0i} + \frac{\bar{m}-1}{\bar{m}}b_{1i} + \frac{\bar{m}-1}{\bar{m}}\frac{\bar{m}-2}{\bar{m}}b_{2i} \tag{29}$$

Where $a_{0i}, a_{1i}, a_{2i}, b_{0i}, b_{1i}, b_{2i}$ are constants [38].

C_1 is defined as:

$$C_1 = \left(1 + Z^{hc} + \rho\frac{\partial Z^{hc}}{\partial\rho}\right)^{-1} = \left(1 + \bar{m}\frac{8\eta - 8\eta^2}{(1-\eta)^4} + (1-\bar{m})\frac{20\eta - 27\eta^2 + 12\eta^3 - 2\eta^4}{[(1-\eta)(2-\eta)]^2}\right)^{-1} \tag{30}$$

The terms $\overline{m^2\varepsilon\sigma_d^3}$ and $\overline{m^2\varepsilon^2\sigma_d^3}$ are defined as:

$$\overline{m^2\varepsilon\sigma_d^{\,3}} = \sum_i^{nc}\sum_j^{nc} x_i x_j m_i m_j \left(\frac{\varepsilon_{ij}}{kT}\right)\sigma_{ij}^3 \tag{31}$$

$$\overline{m^2\varepsilon^2\sigma_d^{\,3}} = \sum_i^{nc}\sum_j^{nc} x_i x_j m_i m_j \left(\frac{\varepsilon_{ij}}{kT}\right)^2 \sigma_{ij}^3 \tag{32}$$

Compressibility factor

Then the compressibility factor is calculated as the sum of the ideal gas contribution (considered to be 1), the dispersion contribution and the residual hard-chain contribution [38]:

$$Z = 1 + Z^{hc} + Z^{disp} \tag{33}$$

$$Z^{hs} = \frac{\varsigma_3}{(1-\varsigma_3)} + \frac{3\varsigma_1\varsigma_2}{\varsigma_0(1-\varsigma_3)^2} + \frac{3\varsigma_2^3 - \varsigma_3\varsigma_2^3}{\varsigma_0(1-\varsigma_3)^3} \tag{34}$$

$$Z^{hc} = \bar{m}Z^{hs} - \sum_i x_i(m_i - 1)(g_{ii}^{hs})^{-1}\rho_m \frac{\partial g_{ii}^{hs}}{\partial \rho_m} \tag{35}$$

$$Z^{disp} = -2\pi\rho_m \frac{\partial(\eta I_1)}{\partial \eta}\overline{m^2\varepsilon\sigma_d^{\,3}} - \pi\rho_m\bar{m}\left[C_1\frac{\partial(\eta I_2)}{\partial\eta} + C_2\eta I_2\right]\overline{m^2\varepsilon^2\sigma_d^{\,3}} \tag{36}$$

where:

$$C_2 = \frac{\partial C_1}{\partial \eta} = -C_1^2\left(\bar{m}\frac{-4\eta^2+20\eta+8}{(1-\eta)^5} + (1-\bar{m})\frac{2\eta^3+12\eta^2-48\eta+40}{\left[(1-\eta)(2-\eta)\right]^3}\right) \tag{37}$$

$$\rho\frac{\partial g_{ij}^{hs}}{\partial\rho} = \frac{\zeta_3}{(1-\zeta_3)^2} + \left(\frac{d_i d_j}{d_i + d_j}\right)\left(\frac{3\zeta_2}{(1-\zeta_3)^2} + \frac{6\zeta_2\zeta_3}{(1-\zeta_3)^3}\right) + \left(\frac{d_i d_j}{d_i + d_j}\right)^2\left(\frac{4\zeta_2^{\,2}}{(1-\zeta_3)^3} + \frac{6\zeta_2^{\,2}\zeta_3}{(1-\zeta_3)^4}\right) \tag{38}$$

$$\frac{\partial(\eta I_1)}{\partial\eta} = \sum_{j=0}^{6} a_j(\bar{m})(j+1)\eta^i \tag{39}$$

$$\frac{\partial(\eta I_2)}{\partial\eta} = \sum_{j=0}^{6} b_j(\bar{m})(j+1)\eta^i \tag{40}$$

Derivative of the Helmholtz free energy respect to temperature.

The temperature derivative of $\tilde{a}^{res}$ is the sum of two contributions.

$$\left(\frac{\partial \tilde{a}^{res}}{\partial T}\right)_{\rho,x_i} = \left(\frac{\partial \tilde{a}^{hc}}{\partial T}\right)_{\rho,x_i} + \left(\frac{\partial \tilde{a}^{disp}}{\partial T}\right)_{\rho,x_i} \tag{41}$$

The temperature derivative of the Helmholtz free energy hard-chain reference contribution is:

$$\left(\frac{\partial \tilde{a}^{hc}}{\partial T}\right)_{\rho,x_i} = \bar{m}\left(\frac{\partial \tilde{a}^{hs}}{\partial T}\right)_{\rho,x_i} - \sum_i x_i (m_i - 1)(g_{ii}{}^{hs})^{-1}\left(\frac{\partial g_{ii}{}^{hs}}{\partial T}\right)_{\rho,x_i} \tag{42}$$

The temperature derivative of the Helmholtz free energy residual contribution of the hard-sphere system is:

$$\left(\frac{\partial \tilde{a}^{hs}}{\partial T}\right)_{\rho,x_i} = \frac{1}{\varsigma_0}\left[\begin{array}{l}\dfrac{3\left(\varsigma_{1,T}\varsigma_2 + \varsigma_1\varsigma_{2,T}\right)}{\left(1-\varsigma_3\right)} + \dfrac{3\varsigma_1\varsigma_2\varsigma_{3,T}}{\left(1-\varsigma_3\right)^2} + \dfrac{3{\varsigma_2}^2\varsigma_{2,T}}{\varsigma_3\left(1-\varsigma_3\right)^2} + \dfrac{{\varsigma_2}^3\varsigma_{3,T}\left(3\varsigma_3-1\right)}{{\varsigma_3}^2\left(1-\varsigma_3\right)^3} + \\ \left(\dfrac{3{\varsigma_2}^2\varsigma_{2,T}\varsigma_3 - 2{\varsigma_2}^3\varsigma_{3,T}}{{\varsigma_3}^3}\right)\ln\left(1-\varsigma_3\right) + \left(\varsigma_0 - \dfrac{{\varsigma_2}^3}{{\varsigma_3}^2}\right)\dfrac{\varsigma_{3,T}}{\left(1-\varsigma_3\right)}\end{array}\right] \tag{43}$$

with abbreviations for two temperature derivatives:

$$\varsigma_{n,T} = \frac{\partial \varsigma_n}{\partial T} = \frac{\pi}{6}\rho\sum_i x_i m_i n d_{i,T}(d_i)^{n-1} \qquad n \in \{0,1,2,3\} \tag{44}$$

$$d_{i,T} = \frac{\partial d_i}{\partial T} = \sigma_i\left(3\frac{\varepsilon_i}{kT^2}\right)\left[-0.12\exp\left(-3\frac{\varepsilon_i}{kT}\right)\right]$$

The temperature derivative of the radial pair distribution function is:

$$\begin{array}{l}\dfrac{\partial g_{ii}^{hs}}{\partial T} = \dfrac{\varsigma_{3,T}}{(1-\varsigma_3)^2} + \left(\dfrac{1}{2}d_{i,T}\right)\dfrac{\varsigma_2}{(1-\varsigma_3)^2} + \left(\dfrac{1}{2}d_i\right)\left(\dfrac{3\varsigma_{2,T}}{(1-\varsigma_3)^2} + \dfrac{6\varsigma_2\varsigma_{3,T}}{(1-\varsigma_3)^3}\right) + \\ \left(\dfrac{1}{2}d_i d_{i,T}\right)\dfrac{2{\varsigma_2}^2}{(1-\varsigma_3)^3} + \left(\dfrac{1}{2}d_i\right)^2\left(\dfrac{4\varsigma_2\varsigma_{2,T}}{(1-\varsigma_3)^3} + \dfrac{6{\varsigma_2}^2\varsigma_{3,T}}{(1-\varsigma_3)^4}\right)\end{array} \tag{45}$$

The temperature derivative of the Helmholtz free energy contribution due to dispersive attraction is:

$$\begin{array}{l}\left(\dfrac{\partial \tilde{a}^{disp}}{\partial T}\right)_{\rho,x_i} = -2\pi\rho\left(\dfrac{\partial I_1}{\partial T} - \dfrac{I_1}{\partial T}\right)\overline{m^2\varepsilon{\sigma_d}^3} - \pi\rho\bar{m} \\ \left[\dfrac{\partial C_1}{\partial T}I_2 + C_1\dfrac{\partial I_2}{\partial T} - 2C_1\dfrac{I_2}{T}\right]\overline{m^2\varepsilon^2{\sigma_d}^3}\end{array} \tag{46}$$

with

$$\frac{\partial I_1}{\partial T} = \sum_{i=0}^{6} a_i(\overline{m}) i \varsigma_{3,T} \eta^{i-1} \tag{47}$$

$$\frac{\partial I_2}{\partial T} = \sum_{i=0}^{6} b_i(\overline{m}) i \varsigma_{3,T} \eta^{i-1} \tag{48}$$

$$\frac{\partial C_1}{\partial T} = \varsigma_{3,T} C_2 \tag{49}$$

Estimation of enthalpy and sound speed.

The enthalpy is used to compute the thermal diffusion vector in the parabolic sub-step. It is computed as the sum of the ideal contribution (obtained by integrating the ideal heat capacity at constant pressure with respect to the temperature) and the residual enthalpy [38]:

$$\frac{\hat{h}^{res}}{RT} = -T\left(\frac{\partial \tilde{a}^{res}}{\partial T}\right)_{\rho,x_i} + (Z-1) \tag{50}$$

Sound speed is computed using the equation applied by [47]:

$$c = \sqrt{\frac{C_p}{C_v}\left(\frac{\partial P}{\partial \rho_m}\right)_T} \tag{51}$$

where C_p and C_v are the heat capacities at constant pressure and volume respectively [39].

The derivatives needed to compute the sound speed are:

$$\left(\frac{\partial P}{\partial \rho_m}\right)_{T,x_i} = \left(\frac{\partial P}{\partial \eta}\right)_{T,x_i}\left(\frac{\partial \eta}{\partial \rho_m}\right)_{T,x_i} \tag{52}$$

$$\left(\frac{\partial \eta}{\partial \rho_m}\right)_{T,x_i} = \frac{\pi}{6}\left(\sum_i x_i m_i d_i^3\right) \tag{53}$$

$$\left(\frac{\partial P}{\partial \eta}\right)_{T,x_i} = k_B T\left(10^{10}\right)^3\left[\rho_m\left(\frac{\partial Z}{\partial \eta}\right)_{T,x_i} + Z\left(\frac{\partial \rho_m}{\partial \eta}\right)_{T,x_i}\right] \tag{54}$$

$$\left(\frac{\partial \rho_m}{\partial \eta}\right)_{T,x_i} = \frac{6}{\pi}\left(\sum_i x_i m_i d_i^3\right)^{-1} \tag{55}$$

$\left(\frac{\partial Z}{\partial \eta}\right)_{T,x_i}$ can be found in [48]. (56)

Appendix B Hyperbolicity of Euler system with PC-SAFT EoS

The hyperbolicity of the Euler system relies on a real speed of sound [3]. Using the PC-SAFT, the speed of sound is always real outside of the vapor-liquid equilibrium state. Inside the vapor-liquid equilibrium region, the spinodal curves (determined by $\left(\partial p / \partial v\right)_T = 0$) enclose the unstable / non-convex region where a complex speed of sound could be found, see Figure 22.

Appendix C Pressure-composition phase diagram for the N_2+$C_{12}H_{26}$ system

The calculation of the number of phases present in a mixture in a certain condition is a recognized problem in the utilization of any EoS. In some cases, the number of phases is assumed a priori and then the composition in every phase is calculated by imposing equilibrium conditions. However, this technique often leads to divergence in the iterative methods used to achieve these. In our case, this is solved by an isothermal flash calculation after a stability analysis using the Tangent Plane Criterion Method proposed by [49] and applied to the PC-SAFT EoS by [50], see Figure 23.

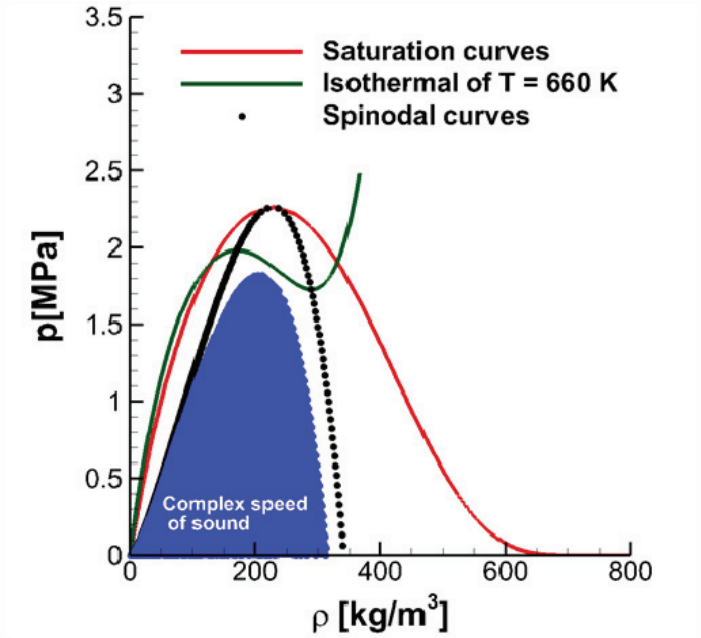

Figure 22. The vapor dome, non-convex region and the region with complex speed of sound of dodecane computed using the PC-SAFT EoS.

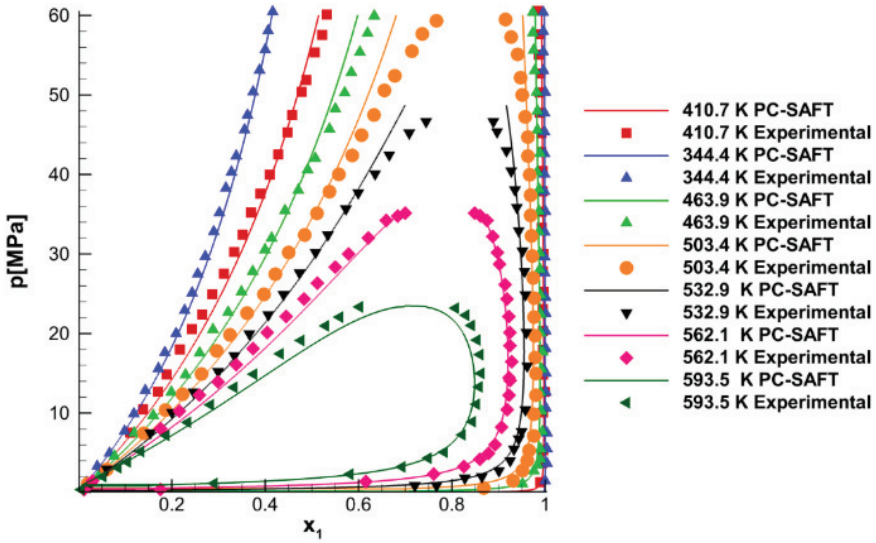

Figure 23. Experimental [51] and calculated pressure-composition phase diagram for the N_2 (1) + $C_{12}H_{26}$ (2) system. Solid lines: PC-SAFT EoS with k_{ij} = 0.144

Appendix D PC-SAFT EoS subroutines

Algorithm 1: Fully conservative formulation

Inputs:
- From conservative variables: ρ, e, Y_i
- Temperature from the previous time step
- Specific values of each component: $\sigma, \varepsilon / K, k_{ij}, m$

Algorithm:

1) Compute the mole fraction of each component

DO

if $\left[\left(\text{abs (e(CSV)-e(PC-SAFT)}\right) > 0.001\right]$ *then*

2) Compute segment diameter of each component (eq.21)
3) Compute mean segment number (eq.17)
4) Compute the coefficients a_i and b_i (eq.28-29)
5) Compute abbreviations (eq.31-32)
5) Compute ζ_n (eq.19)
6) Compute radial distribution function of the hard sphere fluid (eq.24)
7) Compute contribution of the hard sphere fluid to the compressibility factor (eq.34)
8) Compute contribution of the hard chain to the compressibility factor (eq.35)
9) Compute dispersion contribution to the compressibility factor (eq.36)
10) Compute total compressibility (eq.33)
11) Compute pressure (eq.8)
12) Compute partial derivative of the Helmholtz free energy respect to temperature
13) Compute residual internal energy
14) Compute residual enthalpy
15) Compute sonic fluid velocity
16) Compute ideal enthalpy
17) Compute ideal internal energy
18) Compute total enthalpy
19) Compute total internal energy
20) Compute the new temperature using the Newton-Raphson method. The temperature dependent function used is the internal energy

ELSE

RETURN

END IF

END DO

Algorithm 2: Quasi-conservative formulation

Algorithm

Inputs
- From conservative variables: ρ, Y_i
- From double flux model: p
- Temperature from the previous time step
- Specific values of each component: $\sigma, \varepsilon / K, k_{ij}, m$

1) Compute the mole fraction of each component

DO

if $\left[\left(\text{abs (p(double flux model)-p(PC-SAFT)}\right) > 0.001\right]$ *then*

2) Compute segment diameter of each component (eq.21)
3) Compute mean segment number (eq.17)
4) Compute the coefficients a_i and b_i (eq.28-29)
5) Compute abbreviations (eq.31-32)
5) Compute ζ_n (eq.19)
6) Compute radial distribution function of the hard sphere fluid (eq.24)
7) Compute contribution of the hard sphere fluid to the compressibility factor (eq.34)
8) Compute contribution of the hard chain to the compressibility factor (eq.35)
9) Compute dispersion contribution to the compressibility factor (eq.36)
10) Compute total compressibility (eq.33)
11) Compute pressure (eq.8)
12) Compute partial derivative of the Helmholtz free energy respect to temperature
13) Compute residual internal energy
14) Compute residual enthalpy
15) Compute sonic fluid velocity
16) Compute ideal enthalpy
17) Compute ideal internal energy
18) Compute total enthalpy
19) Compute total internal energy
20) Compute the new temperature using the Newton-Raphson method. The temperature dependent function used is the pressure

ELSE

RETURN

END IF

END DO

References

[1] S. Ashley, "Supercritical fuel injection and combustion," *SAE article*, 2010.

[2] J. Matheis and S. Hickel, "Multi-component vapor-liquid equilibrium model for LES of high-pressure fuel injection and application to ECN Spray A," *Int. J. Multiph. Flow*, vol. 99, pp. 294–311, 2017.

[3] P. C. Ma, Y. Lv, and M. Ihme, "An entropy-stable hybrid scheme for simulations of transcritical real-fluid flows," *J. Comput. Phys.*, vol. 340, no. March, pp. 330–357, 2017.

[4] H. Terashima and M. Koshi, "Approach for simulating gas-liquid-like flows under supercritical pressures using a high-order central differencing scheme," *J. Comput. Phys.*, vol. 231, no. 20, pp. 6907–6923, 2012.

[5] P. C. Ma and M. Ihme, "ILASS-Americas 29th Annual Conference on Liquid Atomization and Spray Systems, Atlanta, GA, May 2017," no. May, 2017.

[6] J. C. Oefelein and V. Yang, "Modeling High-Pressure Mixing and Combustion Processes in Liquid Rocket Engines," *J. Propuls. Power*, vol. 14, no. 5, pp. 843–857, 1998.

[7] N. Zong, H. Meng, S. Y. Hsieh, and V. Yang, "A numerical study of cryogenic fluid injection and mixing under supercritical conditions," *Phys. Fluids*, vol. 16, no. 12, pp. 4248–4261, 2004.

[8] L. Selle and T. Schmitt, "Large-Eddy Simulation of Single-Species Flows Under Supercritical Thermodynamic Conditions," *Combust. Sci. Technol.*, vol. 182, no. 4–6, pp. 392–404, 2010.

[9] J.-P. Hickey and M. Ihme, "Supercritical mixing and combustion in rocket propulsion," no. Chehroudi 2012, pp. 21–36, 2013.

[10] G.-S. Jiang and C.-W. Shu, "Efficient Implementation of Weighted ENO Schemes," *J. Comput. Phys.*, vol. 126, no. 1, pp. 202–228, 1996.

[11] H. J. Berg, R. I. D, D.-Y. Peng, and D. B. Robinson, "A New Two-Constant Equation of State," *J. Ind. fng. Chem. J. Phys. Chem. Ind. fng. Chem.. Fundam. J. Agric. Sci. Van Stralen, S. J. 0.. lnt. J. Heat Mass Transf. I O*, vol. 51, no. 107, pp. 385–1082, 1972.

[12] G. Soave, "Equilibrium constants from a modified Redlich-Kwong equation of state," *Chem. Eng. Sci.*, 1972.

[13] H. Terashima, S. Kawai, and N. Yamanishi, "High-Resolution Numerical Method for Supercritical Flows with Large Density Variations," *AIAA J.*, vol. 49, no. 12, pp. 2658–2672, 2011.

[14] H. Terashima and M. Koshi, "Characterization of cryogenic nitrogen jet mixings under supercritical pressures," *51st AIAA Aerosp. Sci. Meet. Incl. New Horizons Forum Aerosp. Expo. 2013*, no. January, pp. 2–11, 2013.

[15] H. Terashima and M. Koshi, "Strategy for simulating supercritical cryogenic jets using high-order schemes," *Comput. Fluids*, vol. 85, pp. 39–46, 2013.

[16] J.-P. Hickey, P. C. Ma, M. Ihme, and S. Thakur, "Large Eddy Simulation of Shear Coaxial Rocket Injector: Real Fluid Effects."

[17] P. C. Ma, L. Bravo, and M. Ihme, "Supercritical and transcritical real-fluid mixing in diesel engine applications," 2014, pp. 99–108.

[18] M. S. Wertheim, "Fluids with highly directional attractive forces.I. Statistical thermodynamics," *J. Stat. Phys.*, vol. 35, no. 1–2, pp. 19–34, 1984.

[19] M. S. Wertheim, "Fluids with highly directional attractive forces. II. Thermodynamic perturbation theory and integral equations," *J. Stat. Phys.*, vol. 35, no. 1–2, pp. 35–47, 1984.

[20] M. S. Wertheim, "Fluids with highly directional attractive forces. III. Multiple attraction sites," *J. Stat. Phys.*, vol. 42, no. 3–4, pp. 459–476, 1986.

[21] M. S. Wertheim, "Fluids with Highly Directional Attractive Forces . IV . Equilibrium Polymerization," vol. 42, pp. 477–492, 1986.

[22] W. G. Chapman, K. E. Gubbins, G. Jackson, and M. Radosz, "SAFT: Equation-of-

state solution model for associating fluids," *Fluid Phase Equilib.*, vol. 52, no. C, pp. 31–38, 1989.

[23] W. G. Chapman, G. Jackson, and K. E. Gubbins, "Phase equilibria of associating fluids," *Mol. Phys.*, vol. 65, no. 5, pp. 1057–1079, Dec. 1988.

[24] N. Khare Prasad, "Predictive Modeling of Metal-Catalyzed Polyolefin Processes," 2003.

[25] S. Leekumjorn and K. Krejbjerg, "Phase behavior of reservoir fluids: Comparisons of PC-SAFT and cubic EOS simulations," *Fluid Phase Equilib.*, vol. 359, pp. 17–23, 2013.

[26] A. J. de Villiers, C. E. Schwarz, A. J. Burger, and G. M. Kontogeorgis, "Evaluation of the PC-SAFT, SAFT and CPA equations of state in predicting derivative properties of selected non-polar and hydrogen-bonding compounds," *Fluid Phase Equilib.*, vol. 338, pp. 1–15, 2013.

[27] M. Salimi and A. Bahramian, "The prediction of the speed of sound in hydrocarbon liquids and gases: The Peng-Robinson equation of state versus SAFT-BACK," *Pet. Sci. Technol.*, vol. 32, no. 4, pp. 409–417, 2014.

[28] K. S. Pedersen and C. H. Sørensen, "PC-SAFT Equation of State Applied to Petroleum Reservoir Fluids," *SPE Annu. Tech. Conf. Exhib.*, vol. 1, no. 4, pp. 1–10, 2007.

[29] X. Liang, B. Maribo-Mogensen, K. Thomsen, W. Yan, and G. M. Kontogeorgis, "Approach to improve speed of sound calculation within PC-SAFT framework," *Ind. Eng. Chem. Res.*, vol. 51, no. 45, pp. 14903–14914, 2012.

[30] T. Schmitt, L. Selle, A. Ruiz, and B. Cuenot, "Large-Eddy Simulation of Supercritical-Pressure Round Jets," *AIAA J.*, vol. 48, no. 9, pp. 2133–2144, 2010.

[31] R. Abgrall and S. Karni, "Computations of compressible multifluids," *J. Comput. Phys.*, vol. 169, pp. 594–623, 2001.

[32] G. Billet and R. Abgrall, "An adaptive shock-capturing algorithm for solving unsteady reactive flows," *Comput. Fluids*, vol. 32, no. 10, pp. 1473–1495, 2003.

[33] P. C. Ma, Y. Lv, and M. Ihme, "Numerical methods to prevent pressure oscillations in transcritical flows," no. 1999, pp. 1–12, 2017.

[34] R. W. Houim and K. K. Kuo, "A low-dissipation and time-accurate method for compressible multi-component flow with variable specific heat ratios," *J. Comput. Phys.*, vol. 230, no. 23, pp. 8527–8553, 2011.

[35] R. J. Spiteri and S. J. Ruuth, "A New Class of Optimal High-Order Strong-Stability-Preserving Time Discretization Methods," *SIAM J. Numer. Anal.*, vol. 40, no. 2, pp. 469–491, 2002.

[36] T. H. Chung, M. Ajlan, L. L. Lee, and K. E. Starling, "Generalized multiparameter correlation for nonpolar and polar fluid transport properties," *Ind. Eng. Chem. Res.*, vol. 27, no. 4, pp. 671–679, Apr. 1988.

[37] M. R. Riazi and C. H. Whitson, "Estimating diffusion coefficients of dense fluids," *Ind. Eng. Chem. Res.*, vol. 32, no. 12, pp. 3081–3088, 1993.

[38] J. Gross and G. Sadowski, "Perturbed-Chain SAFT: An Equation of State Based on a Perturbation Theory for Chain Molecules," *Ind. Eng. Chem. Res.*, vol. 40, no. 4, pp. 1244–1260, 2001.

[39] M. Farzaneh-Gord, M. Roozbahani, H. R. Rahbari, and S. J. Haghighat Hosseini, "Modeling thermodynamic properties of natural gas mixtures using perturbed-chain statistical associating fluid theory," *Russ. J. Appl. Chem.*, vol. 86, no. 6, pp. 867–878, 2013.

[40] E. W. Lemmon, M. L. Huber, and M. O. McLinden, "NIST reference fluid thermodynamic and transport properties–REFPROP." version, 2002.

[41] N. Kyriazis, P. Koukouvinis, and M. Gavaises, "Numerical investigation of bubble dynamics using tabulated data," *Int. J. Multiph. Flow*, vol. 93, no. Supplement C, pp. 158–177, 2017.

[42] D. T. Banuti, P. C. Ma, and M. Ihme, "Phase separation analysis in supercritical injection using large-eddy simulation and vapor-liquid equilibrium," *53rd*

AIAA/SAE/ASEE Jt. Propuls. Conf. 2017, no. July, 2017.

[43] S. Kawai and H. Terashima, "A high-resolution scheme for compressible multicomponent flows with shock waves," *Int. J. Numer. Methods Fluids*, vol. 66, no. 10, pp. 1207–1225, Aug. 2011.

[44] P. C. Ma, H. Wu, D. T. Banuti, and M. Ihme, "Numerical analysis on mixing processes for transcritical real-fluid simulations," *2018 AIAA Aerosp. Sci. Meet.*, no. January, 2018.

[45] J. M. H. L. Sengers and E. Kiran, *Supercritical Fluids: Fundamentals for Application*. Kluwer Academic Publishers, 1994.

[46] G. Lacaze, A. Misdariis, A. Ruiz, and J. C. Oefelein, "Analysis of high-pressure Diesel fuel injection processes using LES with real-fluid thermodynamics and transport," *Proc. Combust. Inst.*, vol. 35, no. 2, pp. 1603–1611, 2015.

[47] N. Diamantonis and I. Economou, "Evaluation of SAFT and PC-SAFT EoS for the calculation of thermodynamic derivative properties of fluids related to carbon capture and sequestration," no. June 2011, pp. 1–32, 2011.

[48] R. Privat, R. Gani, and J. N. Jaubert, "Are safe results obtained when the PC-SAFT equation of state is applied to ordinary pure chemicals?," *Fluid Phase Equilib.*, vol. 295, no. 1, pp. 76–92, 2010.

[49] M. L. Michelsen, "THE ISOTHERMAL FLASH PROBLEM. PART I. STABILITY," *Fluid Phase Equilib.*, vol. 9, 1982.

[50] and A. R. Justo-García, Daimler N., Fernando García-Sánchez, "Isothermal multiphase flash calculations with the PC-SAFT equation of state," in *AIP Conference Proceedings*, 2008, vol. 979, pp. 195–214.

[51] D. N. Justo-garcía, B. E. García-flores, and F. García-s, "Vapor - Liquid Equilibrium Data for the Nitrogen þ Dodecane System at Temperatures from (344 to 593) K and at Pressures up to 60 MPa," pp. 1555–1564, 2011.